Semiempirical Local Spin: Theory and Implementation of the ZILSH Method for Predicting Heisenberg Exchange Constants of Polynuclear Transition Metal Complexes

TED A. O'BRIEN,[*] ERNEST R. DAVIDSON[†]

Department of Chemistry, Indiana University, Bloomington, IN 47405-7102

Received 9 May 2002; accepted 15 October 2002

DOI 10.1002/qua.10513

ABSTRACT: The local spin formalism (Clark, A. E.; Davidson, E. R. J Chem Phys 2001, 115, 7382–7392) for computing expectation values $\langle S_A \cdot S_B \rangle$ that appear in the Heisenberg spin model has been extended to semiempirical single determinant wave functions. An alternative derivation of expectation values in restricted and unrestricted cases is given that takes advantage of the zero differential overlap (ZDO) approximation. A formal connection between single determinant wave functions (which are not in general spin eigenfunctions) and the Heisenberg spin model was established by demonstrating that energies of single determinants that are eigenfunctions of the local spin operators with eigenvalues corresponding to high-spin radical centers are given by the same Heisenberg coupling constants $\{J_{AB}\}$ that describe the true spin states of the system. Unrestricted single determinant wave functions for transition metal complexes are good approximations of local spin eigenfunctions when the metal *d* orbitals are local in character and all unpaired electrons on each metal have the same spin (although spins on different metals might be reversed). Good approximations of the coupling constants can then be extracted from local spin expectation values $\langle S_A \cdot S_B \rangle$ energies of the single determinant wave functions. Once the coupling constants are obtained, diagonalization of the Heisenberg spin Hamiltonian provides predictions of the energies and compositions of the spin states. A computational method is presented for obtaining coupling constants and spin-state energies in this way for polynuclear

Correspondence to: T. O'Brien; e-mail: teobrien@indiana.edu

[*]Present address: Department of Chemistry, Indiana University–Purdue University Indianapolis, Indianapolis, IN 46202-3274.

[†]Present address: Department of Chemistry, University of Washington, Seattle, WA 98195-1700.

International Journal of Quantum Chemistry, Vol 92, 294–325 (2003)

transition metal complexes using the intermediate neglect of differential overlap Hamiltonian parameterized for optical spectroscopy (INDO/S) in the ZINDO program. This method is referred to as ZILSH, derived from ZINDO, Davidson's local spin formalism, and the Heisenberg spin model. Coupling constants and spin ground states obtained for 10 iron complexes containing from 2 to 6 metals are found to agree well with experimental results in most cases. In the case of the complex $[Fe_6O_3(OAc)_9(OEt)_2(bpy)_2]^+$, *a priori* predictions of the coupling constants yield a ground-state spin of zero, in agreement with variable-temperature magnetization data, and corroborate spin alignments proposed earlier on the basis of structural considerations. This demonstrates the potential of the ZILSH method to aid in understanding magnetic interactions in polynuclear transition metal complexes.
 Int J Quantum Chem 92: 294–325, 2003

Key words: Heisenberg spin model; single determinant wave functions; zero differential overlap; transition metal complexes

1. Introduction

Molecules with nonzero spin magnetic moments are ubiquitous throughout chemistry. In particular, the properties and applications of complexes containing multiple magnetic transition metal ions have made them a focus of study across the subfields of chemistry. For example, many have novel optical and magnetic properties of potential use in molecular-level computing devices. An exciting class of such complexes are the single-molecule magnets, which display slow reversal of their spin magnetic moments (SMMs) at low temperature. As the name implies, these so-called SMMs are in effect molecular-scale magnets and hence display quantum magnetization behavior. They are thus being studied for fundamental as well as practical reasons. Another important area in which polynuclear complexes are relevant is biochemistry. The biologically important process of nitrogen fixation, for example, is mediated by the enzyme nitrogenase, which has a cofactor containing multiple iron ions. Another example is the water oxidation complex (WOC) of the photosynthetic reaction center, which contains a tetranuclear manganese active site. Many other biochemical reactions are also mediated by proteins or enzymes with active sites containing radical metal ions.

There can be convergence between the two seemingly unrelated areas of biologic chemistry and molecular-scale magnetic behavior. This is the case with complexes containing the $[Mn_4O_3X]^{+6}$ core. These complexes were originally investigated as synthetic analogs of the WOC, but were later found to also be SMMs [1, 2]. This perhaps indicates the common importance of the open-shell character of the complexes to their properties and reaction chemistries. It is therefore vital to continue to develop further understanding of spin couplings in such complexes. Unfortunately, complexes of this type are difficult to treat with the methods of quantum chemistry. Their large size and the complicated electronic structure associated with multiple open-shell transition metals makes them one of the toughest challenges for theoretical methods. Further development of methods that can successfully treat large transition metal complexes and active sites is thus important. This article describes a method for treating spin couplings in large polynuclear transition metal complexes, based on a new synthesis of semiempirical quantum chemistry and the Heisenberg spin Hamiltonian (HSH).

1.1. HEISENBERG SPIN HAMILTONIAN

For many years the energies of the spin states of molecules with multiple radical centers or fragments have been described by the HSH,

$$\hat{H} = -\sum_{A<B} J_{AB} S_A \cdot S_B. \tag{1}$$

Here, A, B, ... are radical centers, S_A is the spin assumed to be localized to the center (or fragment) labeled with A, and J_{AB} is the so-called Heisenberg coupling constant. For simple biradical cases, this Hamiltonian provides a ladder of eigenenergies for the spin states in which the energy either increases or decreases as the total spin quantum number increases, depending on the nature of the coupling. J_{AB} can be negative, with the state of lowest total spin lowest in energy, or positive, with the state of highest total spin lowest in energy. These two cases

are termed antiferromagnetic or ferromagnetic, respectively. In complexes with multiple radical centers, ground states with spins intermediate between the ferromagnetic and antiferromagnetic values can be obtained, depending on the relative magnitudes and directions of the various exchange interactions. In some cases there is competition between different exchange pathways, which is known as "spin frustration."

The Heisenberg spin model (HSM) assumes that the radical centers each have a well-defined local spin quantum number, and that these spins are coupled to form states with well-defined total spin quantum numbers. Further, the total spin has a well-defined quantum number for the z component of spin. The eigenstates assumed by the HSM can thus be denoted as $|S\ S_z\ S_A\ S_B \cdots\rangle$, and the following eigenvalue equations are taken to apply:

$$\hat{S}^2|S\ S_z\ S_A\ S_B \cdots\rangle = S(S+1)|S\ S_z\ S_A\ S_B \cdots\rangle \quad (2)$$

$$\hat{S}_z|S\ S_z\ S_A\ S_B \cdots\rangle = S_z|S\ S_z\ S_A\ S_B \cdots\rangle \quad (3)$$

$$\hat{S}_A^2|S\ S_z\ S_A\ S_B \cdots\rangle = S_A(S_A+1)|S\ S_z\ S_A\ S_B \cdots\rangle. \quad (4)$$

Each state with total spin quantum number S has $2S + 1$ components with different values of S_z ranging from S to $-S$. In the absence of zero-field splitting or an external magnetic field these components have the same energy, so we consider only those components with $S_z = S$. The various possible values of the quantum numbers S_{zA}, S_{zB}, ... must be considered, however, because $S_Z = S_{zA} + S_{zB} + \cdots$. Beyond this requirement that S_{zA}, S_{zB}, ... sum to give S_Z, the local z components of spin do not in general take on well-defined quantum numbers in eigenfunctions of the HSH.

The spin operators in Eq. (1) may be recast in terms of raising and lowering operators for each local spin, transforming the HSH into

$$\hat{H} = -\frac{1}{2}\sum_{A<B} J_{AB}(S_A^+S_B^- + S_A^-S_B^+ + 2S_{zA}\cdot S_{zB}). \quad (5)$$

The basis functions for this operator are thus $|S_AS_{zA}\rangle|S_BS_{zB}\rangle\cdots|S_NS_{zN}\rangle$ (henceforth referred to as "components"), and the eigenstates $|S\ S_z\ S_A\ S_B \cdots S_N\rangle$ are linear combinations of these basis functions,

$$|S\ S_z\ S_A\ S_B \cdots\rangle = \sum_{S_{zA},S_{zB},\ldots} C^{S,S_z}_{S_{zA},S_{zB},\ldots}|S_AS_{zA}\rangle|S_BS_{zB}\rangle\cdots. \quad (6)$$

The expansion coefficients in Eq. (6) would be equivalent to Clebsch–Gordon coefficients for coupling of angular momenta if not for the presence of the $\{J_{AB}\}$ in Eqs. (1) and (5). With the exchange parameters present, the operator of Eq. (5) must be diagonalized in the basis of the $\{|S_AS_{zA}\rangle|S_BS_{zB}\rangle\cdots\}$ to yield the spin states $|S\ S_z\ S_A\ S_B \cdots\rangle$. The local spin quantum numbers $\{S_A\}$ are assigned idealized or "formal" values chosen by what might be called "chemical intuition" [3] by assuming all radical character resides locally on the radical centers. Under this assumption the radical centers in a diradical like benzyne each have $S_A = \frac{1}{2}$, high-spin Fe^{+3} ions in a complex have $S_A = \frac{5}{2}$, etc.

Given the foregoing assumptions, values of J_{AB} are often fit to reproduce either experimentally determined quantities or energies computed with theoretical methods based on the nonrelativistic Born–Oppenheimer electronic Hamiltonian. A widely used example of the former is to fit values for the coupling constants that reproduce curves obtained by recording the magnetic susceptibility of the complex as the temperature is varied. This is done by assuming a Boltzmann distribution of populations of the spin states of the complex as determined by the HSM. The coupling constants are varied until the variable-temperature susceptibility data is accurately reproduced. The HSH is usually simplified in doing so by equating certain exchange parameters based on symmetry and neglecting others.

1.2. HEISENBERG SPIN MODEL AND QUANTUM CHEMISTRY

The coupling constants of Eq. (1) might also be obtained with the methods of quantum chemistry, using energies estimated by electronic structure calculations. In practice the electronic wave functions may or may not be spin eigenfunctions, depending on the level of calculation used. Single determinant wave functions such as those used in unrestricted Hartree–Fock (HF) and unrestricted density functional theory (DFT) calculations, for example, are eigenfunctions of the z component of spin, $\hat{S}_z$ of Eq. (3), but are not eigenfunctions of total spin. Nevertheless, the local spins are still assumed to take on values assigned by chemical intuition. It is also assumed that these local spin values are the same

regardless of the resultant total spin. These assumptions are made even though single determinant wave functions meant to approximate these spin states will suffer from varying degrees of spin contamination. The complex $[Fe_2S_2(SH)_4]^{-2}$ is a good example. Cory and Zerner [4] considered unrestricted single determinant (UHF) approximations of the ferromagnetic and antiferromagnetic states. The former, with $S_z = 5$, was found to have an expectation value of the total spin operator, $\langle \hat{S}^2 \rangle$, of 30.0069 [4], close to the formal value of 30 expected for a state with $S = 5$. The antiferromagnetic component with $S_z = 0$, however, was found to have $\langle \hat{S}^2 \rangle = 4.7768$ [4]. Because the local spins must sum to give the total spin according to $\langle \hat{S}^2 \rangle = \Sigma_{A,B} \langle \hat{S}_A \cdot \hat{S}_B \rangle$, it might not in general be true that the local spins take on formal values or retain the same values in wave functions with different amounts of spin contamination.

The preceding discussion illuminates a basic dichotomy between the HSM and the fundamental assumptions of quantum chemistry. The former uses empirical quantities (J_{AB} and $S_A \cdot S_B$) based on atomic coordinates, while the latter uses spin (and other) operators that act on electronic coordinates. These two distinct approaches have been grafted together in virtually all previous treatments by mixing calculated energies with local spin quantum numbers assigned empirical values. A fuller reconciliation of the Heisenberg model with quantum chemistry requires a quantum mechanical operator for $S_A \cdot S_B$ that acts on electronic coordinates. Davidson recently developed such an operator based on projection operators that apportion the electrons of a molecule among the atoms by means of various population analysis schemes [3, 5]. This operator, $\hat{S}_A \cdot \hat{S}_B$, can be used to obtain expectation values $\langle S_A \cdot S_B \rangle$ for single determinant or configuration interaction (CI) wave functions. These expectation values can then be used with calculated energies in a Heisenberg spin formulation. In a later section of this article it is demonstrated that in favorable cases energies and $\langle S_A \cdot S_B \rangle$ values from any level of approximation can be used to obtain accurate estimates of the coupling constants appropriate for the true spin eigenstates of the molecule, regardless of the spin contamination of the approximate wave functions. This is potentially useful for larger molecules, which can be readily described at the HF or DFT levels but are intractable with complete active space models that utilize true spin eigenfunctions.

Many of the interesting cases described by the HSH are large polynuclear transition metal complexes, whether active sites of proteins or clusters with potential materials applications. Complexes of this sort (large and containing multiple transition metals) are difficult to treat with *ab initio* or even DFT methods, so it would be useful to have a semiempirical implementation of the local spin analysis. In this article we report implementation of local spin in the ZINDO program package [6] and application to polynuclear iron complexes containing from two to six metal ions using the INDO/S semiempirical model [7–16]. The results approximately demonstrate the assumptions of the HSM: Local spins are similar to values assigned by chemical intuition and $|\langle S_A \cdot S_B \rangle|$ values change only slightly with S_z of the wave function.

A computational procedure for determining all Heisenberg coupling constants for complexes with an arbitrary number of metal atoms is also described. This new method uses energies and local spin expectation values computed from UHF wave functions to assess the energetics of the radical spin couplings in a complex. Once the coupling constants have been obtained, the energies and compositions of all spin states can be determined using the Heisenberg model. In this way it is possible to correctly predict intermediate spin ground states that are not accessible by spin-adapted methods due to computational limitations. Results found for several polynuclear Fe^{+3} complexes with the INDO/S model are presented below.

The coupling constants obtained by the new method also can be compared to simplifications of the HSH made by grouping some coupling constants according to symmetry and neglecting others. These assumptions are common in the inorganic literature but have not yet often been amenable to *a priori* examination. We propose that the method of determining coupling constants described here could be an important tool for further study of open-shell polynuclear transition metal complexes.

The article is organized as follows: In Section 2, the local spin operator is developed and expressions for matrix elements of single determinant RHF and UHF wave functions under the zero differential overlap (ZDO) approximation [17] are derived. Then, the connection between state energies and spin couplings calculated at the HF level and the HSH is considered in Section 3. A method for obtaining Heisenberg coupling constants from calculations on different spin components of polynuclear transition metal complexes is described in Section 4. The details of the semiempirical method

used and the computer implementation are described in Section 5. Ten iron complexes containing from two to six metals used as test cases are briefly described in Section 6. Results are presented for the complexes in Section 7. Section 8 presents conclusions and possible future directions of this work.

2. Semiempirical Local Spin

Davidson recently defined "local spin" operators that can be used to calculate expectation values of the quantity $S_A \cdot S_B$ that appears in the HSH from a single determinant wave function [3, 5]. The method uses projection operators that apportion electrons to the atoms of a molecule based on a population analysis scheme. Clark and Davidson recently reported a derivation of the operators and expressions for $\langle \hat{S}_A \cdot \hat{S}_B \rangle$ assuming *ab initio* RHF, UHF, and restricted or unrestricted DFT models [3]. The local spin approach has also been extended to configuration interaction wave functions [5]. This article reports a semiempirical implementation of local spin. An alternative derivation of expressions for expectation values $\langle \hat{S}_A \cdot \hat{S}_B \rangle$ is given that is more straightforward when the ZDO approximation [17] is assumed. The approach used is general and could easily be adapted to CI and other correlated wave functions that reduce to a sum over Slater determinants.

A fundamental difference between the HSM and quantum chemistry is that spin is assigned to atoms in the former but is properly taken as an intrinsic property of electrons in the latter. The operator for the total spin of a set of electrons is

$$\hat{S} = \sum_i \hat{S}(i), \tag{7}$$

where (i) refers to electronic coordinates. A "local spin" operator for the spin associated with a particular atom can be defined using projection operators that project out the contribution to the total spin made by electrons in atomic orbitals centered on each atom. This projection operator is denoted as P_A for the atom labeled as atom A. Its exact form is described below. With this notation, the local spin operator of atom A is

$$\hat{S}_A = \sum_i \hat{S}(i) P_A(i). \tag{8}$$

As with all projection operators, the $\{P_A(i)\}$ must be idempotent,

$$P_A(i) P_B(i) = P_A(i) \delta_{AB}, \tag{9}$$

and it must also be true that

$$\sum_A P_A(i) = 1 \tag{10}$$

for the projectors to be well behaved [so that the total number of electrons, $\Sigma_A \Sigma_i P_A(i)$, is correct]. Davidson considered several forms of the projectors based on various methods of population analysis and showed that projectors defined based on the Löwdin scheme [18] meet these requirements [3]. The Löwdin approach is convenient for ZDO methods and is used exclusively in this article. The representation of the projectors in the molecular orbital (MO) basis of a semiempirical model is described in detail later.

With the above definition of $\hat{S}_A$, the total spin operator is then

$$\hat{S} = \sum_A \hat{S}_A \tag{11}$$

and the operator $\hat{S}^2$ is

$$\hat{S}^2 = \sum_A \sum_B \hat{S}_A \cdot \hat{S}_B. \tag{12}$$

Because the operators $\{\hat{S}_A\}$ commute with each other [3, 5], Eq. (12) indicates that $\hat{S}^2$ commutes with all operator products $\hat{S}_A \cdot \hat{S}_B$. Therefore, states with well-defined total spin are also eigenfunctions of the operators $\hat{S}_A \cdot \hat{S}_B$, and

$$\langle \Psi^S | \hat{S}_A \cdot \hat{S}_B | \Psi^{S'} \rangle = \langle \Psi^S | \hat{S}_A \cdot \hat{S}_B | \Psi^S \rangle \delta_{SS'}. \tag{13}$$

According to definition (8) the operators $\hat{S}_A \cdot \hat{S}_B$ are given by

$$\hat{S}_A \cdot \hat{S}_B = \sum_{i,j} \hat{S}(i) \cdot \hat{S}(j) P_A(i) P_B(j). \tag{14}$$

It is convenient to separate this into diagonal (one-electron) and off-diagonal (two-electron) terms as

$$\hat{S}_A \cdot \hat{S}_B = \sum_i \hat{S}^2(i) P_A(i) P_B(i) + \sum_{i<j} \hat{S}(i) \cdot \hat{S}(j) \times [P_A(i) P_B(j) + P_B(i) P_A(j)]. \tag{15}$$

Because $\hat{S}^2(i)$ gives eigenvalue ¾ when it operates on any electron and using Eq. (9), this becomes

$$\hat{S}_A \cdot \hat{S}_B = \frac{3}{4}\,\delta_{AB} \sum_i P_A(i) + \sum_{i<j} \hat{S}(i) \cdot \hat{S}(j)[P_A(i)\,P_B(j) + P_B(i)\,P_A(j)]. \quad (16)$$

Equation (16) is a quantum mechanical operator representation of the quantity $S_A \cdot S_B$ occurring in the HSM. The operator can be used to obtain expectation values $\langle \hat{S}_A \cdot \hat{S}_B \rangle$ for any electronic wave function, regardless of whether or not that wave function is a spin eigenfunction, given a form for the projection operators $\{P_A\}$.

Clark and Davidson presented a general development and implementation of the local spin operator applicable to both wave function and density functional methods [3]. This article is concerned with applying the local spin operator to semiempirical single determinant RHF and UHF wave functions. With this focus on wave function methods, it is convenient to develop the operator using the standard rules for matrix elements of one- and two-electron operators in a basis of Slater determinants [19]. Only diagonal matrix elements are considered here (i.e., the wave function is assumed to be a single determinant) but the approach used could be easily generalized to include off-diagonal matrix elements needed for CI wave functions. An implementation for semiempirical CI wave functions could be the subject of a future publication.

The matrix element of a single determinant orbital wave function over an operator like $\hat{S}_A \cdot \hat{S}_B$ that consists of sums over one- and two-electron operators is

$$\langle \Psi^{\text{S.D.}} | \hat{S}_A \cdot \hat{S}_B | \Psi^{\text{S.D.}} \rangle = \frac{3}{4}\,\delta_{AB} \sum_m \langle m | P_A | m \rangle + \frac{1}{2} \sum_m \sum_n [\langle mn | \hat{S}(1) \cdot \hat{S}(2) [P_A P_B + P_B P_A] | mn \rangle - \langle mn | \hat{S}(1) \cdot \hat{S}(2) [P_A P_B + P_B P_A] | nm \rangle], \quad (17)$$

where the indices m and n refer to spin orbitals of the form

$$\phi_m(i) = \chi_m(i)\alpha(i)$$
$$\phi_{m'}(i) = \chi_{m'}(i)\beta(i). \quad (18)$$

These spin orbitals are assumed to be delocalized molecular orbitals. Because the two-electron part of $\hat{S}_A \cdot \hat{S}_B$ depends on spin, it is convenient to separate the summations in Eq. (17) into sums over α and β spins,

$$\begin{aligned}\langle \hat{S}_A \cdot \hat{S}_B \rangle = \frac{3}{4}\,\delta_{AB} \left[\sum_{m^\alpha=1}^{N^\alpha} \langle m^\alpha | P_A | m^\alpha \rangle + \sum_{m^\beta=1}^{N^\beta} \langle m^\beta | P_A | m^\beta \rangle \right] + \frac{1}{2} \sum_{m^\alpha} \sum_{n^\alpha} [\langle mn | \hat{S}(1) \cdot \hat{S}(2) [P_A P_B + P_B P_A] | mn \rangle \\ - \langle mn | \hat{S}(1) \cdot \hat{S}(2) [P_A P_B + P_B P_A] | nm \rangle] + \frac{1}{2} \sum_{m^\beta} \sum_{n^\beta} [\langle \overline{mn} | \hat{S}(1) \cdot \hat{S}(2) [P_A P_B + P_B P_A] | \overline{mn} \rangle \\ - \langle \overline{mn} | \hat{S}(1) \cdot \hat{S}(2) [P_A P_B + P_B P_A] | \overline{nm} \rangle] + \sum_{m^\alpha} \sum_{n^\beta} [\langle m\bar{n} | \hat{S}(1) \cdot \hat{S}(2) [P_A P_B + P_B P_A] | m\bar{n} \rangle \\ - \langle m\bar{n} | \hat{S}(1) \cdot \hat{S}(2) [P_A P_B + P_B P_A] | \bar{n}m \rangle]. \end{aligned} \quad (19)$$

Here, β and α spins are represented by the presence or absence of a bar over the orbital indices, respectively. Note that the cumbersome notation $m^{\alpha,\beta}$ has been dropped in the two-electron integrals. The manifold (either $\{\chi^\alpha\}$ or $\{\chi^\beta\}$) to which an orbital belongs is now indicated only by the summation index. Thus, "m" might refer to an orbital from either manifold even though we do not require that χ_m^α and χ_m^β be identical, and the summations over m^α and m^β are not in general of the same length.

The spin part of the operators in Eq. (19) is given by

$$\hat{S}(1) \cdot \hat{S}(2) = \hat{S}_z(1)\hat{S}_z(2) + \frac{1}{2}\,\hat{S}^+(1)\hat{S}^-(2) + \frac{1}{2}\,\hat{S}^-(1)\hat{S}^+(2), \quad (20)$$

where $\hat{S}^\pm$ are the usual raising and lowering operators. It is easiest to apply the spin operators first.

They can be applied to the right because the projection operators have nothing to do with spin and hence commute with the spin operators. Many of the resulting terms are zero, for example, the raising and lowering operators always give zero in the first five two-electron summations in Eq. (19), either by direct annihilation or spin integration after the operators are applied. Taking the first two-electron summation in Eq. (19) as an example,

$$\begin{aligned}\frac{1}{2}\sum_{m^\alpha}\sum_{n^\alpha}&\langle mn|\hat{S}_z(1)\hat{S}_z(2)[P_AP_B + P_BP_A]|mn\rangle \\ &= \frac{1}{8}\sum_{m^\alpha}\sum_{n^\alpha}\langle mn|P_AP_B + P_BP_A|mn\rangle \\ &= \frac{1}{4}\sum_{m^\alpha}\sum_{n^\alpha}\langle m|P_A|m\rangle\langle n|P_B|n\rangle \end{aligned} \tag{21}$$

after relabeling the orbital indices in the summations over the operator P_BP_A. Proceeding in similar fashion, Eq. (19) becomes

$$\begin{aligned}\langle \hat{S}_A\cdot\hat{S}_B\rangle &= \frac{3}{4}\delta_{AB}\left[\sum_{m^\alpha}\langle m|P_A|m\rangle + \sum_{m^\beta}\langle m|P_A|m\rangle\right] \\ &+ \frac{1}{4}\sum_{m^\alpha}\sum_{n^\alpha}\langle m|P_A|m\rangle\langle n|P_B|n\rangle - \frac{1}{4}\sum_{m^\alpha}\sum_{n^\alpha}\langle m|P_A|n\rangle \\ &\times \langle n|P_B|m\rangle + \frac{1}{4}\sum_{m^\beta}\sum_{n^\beta}\langle m|P_A|m\rangle\langle n|P_B|n\rangle \\ &- \frac{1}{4}\sum_{m^\beta}\sum_{n^\beta}\langle m|P_A|n\rangle\langle n|P_B|m\rangle - \frac{1}{4}\sum_{m^\alpha}\sum_{n^\beta}\langle m|P_A|m\rangle \\ &- \sum_{m^\alpha}\sum_{n^\beta}\langle m|P_A|n\rangle\langle n|P_B|m\rangle. \end{aligned} \tag{22}$$

The projection operators P_A must now be defined to proceed further. Because these operators are meant to associate electron densities with atoms in a molecule, they in effect perform a population analysis. Davidson considered several possibilities [3, 5], including the Bader [20, 21] and Löwdin schemes [18]. The latter proves convenient for semiempirical implementations that assume the ZDO approximation. Under the Löwdin scheme the matrix element $\langle\chi_m|P_A|\chi_n\rangle$ reduces to a sum over products of MO coefficients $C^\dagger_{m\mu}C_{\mu n}$ for all atomic orbitals ψ_μ centered on atom A in the Löwdin-orthogonalized basis [3]. This is straightforward for a semiempirical wave function because the basis is assumed to be orthogonal under ZDO and can be regarded as equivalent to the Löwdin basis [18]. The matrix elements $\langle\chi_m|P_A|\chi_n\rangle$ are then given by

$$\langle m^{\alpha,\beta}|P_A|n^{\alpha,\beta}\rangle = \sum_{\mu\in A} C^{\alpha,\beta}_{\mu m}C^{\alpha,\beta}_{\mu n} \tag{23}$$

assuming the expansion coefficients are Hermitian. Taking the first double summation in Eq. (22) as an example, we have

$$\begin{aligned}\frac{1}{4}\sum_{m^\alpha}\sum_{n^\alpha}&\langle m|P_A|m\rangle\langle n|P_B|n\rangle \\ &= \frac{1}{4}\sum_{m^\alpha}\sum_{n^\alpha}\sum_{\mu\in A}|C^\alpha_{\mu m}|^2\sum_{\nu\in B}|C^\alpha_{\nu n}|^2. \end{aligned} \tag{24}$$

Introducing the standard definitions of the first-order Fock–Dirac density matrices [19],

$$\begin{aligned}\rho^\alpha_{\mu\nu} &= \sum_{m^\alpha} C^{\alpha\ \dagger}_{\mu m}C^\alpha_{m\nu} \\ \rho^\beta_{\mu\nu} &= \sum_{m^\beta} C^{\beta\ \dagger}_{\mu m}C^\beta_{m\nu} \end{aligned} \tag{25}$$

the summations are the right side of Eq. (24) can be exchanged, giving

$$\begin{aligned}\frac{1}{4}\sum_{m^\alpha}\sum_{n^\alpha}&\langle m|P_A|m\rangle\langle n|P_B|n\rangle \\ &= \frac{1}{4}\sum_{\mu\in A}\sum_{\nu\in B}\sum_{m^\alpha}|C^\alpha_{\mu m}|^2\sum_{n^\alpha}|C^\alpha_{\nu n}|^2 = \frac{1}{4}\sum_{\mu\in A}\sum_{\nu\in B}\rho^\alpha_{\mu\mu}\rho^\alpha_{\nu\nu}. \end{aligned} \tag{26}$$

Equation (22) thus becomes

$$\begin{aligned}\langle \hat{S}_A\cdot\hat{S}_B\rangle &= \frac{3}{4}\delta_{AB}\sum_{\mu\in A}[\rho^\alpha_{\mu\mu} + \rho^\beta_{\mu\mu}] + \frac{1}{4}\sum_{\mu\in A}\sum_{\nu\in B}\rho^\alpha_{\mu\mu}\rho^\alpha_{\nu\nu} \\ &- \frac{1}{4}\sum_{\mu\in A}\sum_{\nu\in B}\rho^\alpha_{\mu\nu}\rho^\alpha_{\mu\nu} + \frac{1}{4}\sum_{\mu\in A}\sum_{\nu\in B}\rho^\beta_{\mu\mu}\rho^\beta_{\nu\nu} \\ &- \frac{1}{4}\sum_{\mu\in A}\sum_{\nu\in B}\rho^\beta_{\mu\nu}\rho^\beta_{\mu\nu} - \frac{1}{4}\sum_{\mu\in A}\sum_{\nu\in B}\rho^\alpha_{\mu\mu}\rho^\beta_{\nu\nu} \\ &- \frac{1}{4}\sum_{\mu\in A}\sum_{\nu\in B}\rho^\beta_{\mu\mu}\rho^\alpha_{\nu\nu} - \sum_{\mu\in A}\sum_{\nu\in B}\rho^\alpha_{\mu\nu}\rho^\beta_{\mu\nu}. \end{aligned} \tag{27}$$

Introducing now the total density matrix ρ^T and spin density matrix ρ^S,

$$\rho^T = \rho^\alpha + \rho^\beta$$
$$\rho^S = \rho^\alpha - \rho^\beta \tag{28}$$

Eq. (27) becomes

$$\langle \hat{S}_A \cdot \hat{S}_B \rangle^{\mathrm{UHF}} = \frac{3}{4}\delta_{AB} \sum_{\mu\in A} \rho^T_{\mu\mu} - \frac{3}{8} \sum_{\mu\in A}\sum_{\nu\in B} |\rho^T_{\mu\nu}|^2 + \frac{1}{8} \sum_{\mu\in A}\sum_{\nu\in B} |\rho^S_{\mu\nu}|^2 + \frac{1}{4} \sum_{\mu\in A} \rho^S_{\mu\mu} \sum_{\nu\in B} \rho^S_{\nu\nu}. \tag{29}$$

In the RHF case $\rho^\alpha = \rho^\beta = 1/2\,\rho^{\mathrm{RHF}}$, so $\rho^S = 0$ and $\rho^T = \rho^{\mathrm{RHF}}$, and

$$\langle \hat{S}_A \cdot \hat{S}_B \rangle^{\mathrm{RHF}} = \frac{3}{4}\delta_{AB} \sum_{\mu\in A} \rho_{\mu\mu} - \frac{3}{8} \sum_{\mu\in A}\sum_{\nu\in B} |\rho_{\mu\nu}|^2. \tag{30}$$

As pointed out before [3], this expression is interesting because under the ZDO approximation the overlap matrix is assumed to be equal to the unit matrix and the quantity $\Sigma_{\mu\in A}\,\Sigma_{\nu\in B}\,|\rho_{\mu\nu}|^2$ is equal to the Wiberg bond order, B_{AB}, between atoms A and B. When $A \neq B$, then, we have

$$\langle \hat{S}_A \cdot \hat{S}_B \rangle^{\mathrm{RHF}}_{A\neq B} = -\frac{3}{8} B_{AB}. \tag{31}$$

A similar relation exists between bond order and $\langle \hat{S}_A \cdot \hat{S}_B \rangle^{\mathrm{UHF}}$. Mayer [22, 23] defined the bond order between two atoms in a UHF wave function as

$$B_{AB} = 2 \sum_{\mu\in A}\sum_{\nu\in B} (|\rho^\alpha_{\mu\nu}|^2 + |\rho^\beta_{\mu\nu}|^2), \tag{32}$$

which occurs in Eq. (30) along with certain additional terms when the spin density is not zero. One such term is the local z-component of spin for each radical center. An operator of this quantity, $\hat{S}_{zA}$, can be defined in the same way that the operator $\hat{S}_A$ was defined [Eq. (8)]:

$$\hat{S}_{zA} = \sum_i \hat{S}_z(i)\, P_A(i). \tag{33}$$

Proceeding as above, this leads to the convenient result that the expectation value for the local z-component of spin for a radical center is equal to half the sum of diagonal elements of the spin density matrix for the orbitals on that center,

$$m_A \equiv \langle \hat{S}_{zA} \rangle^{\mathrm{UHF}} = \frac{1}{2} \sum_{\mu\in A} \rho^S_{\mu\mu}. \tag{34}$$

This quantity is useful for examining on which atoms the unpaired spins reside for a given UHF wave function, and is used in this capacity below. Definition (34) can be used along with definition (32) in Eq. (29) to yield

$$\langle \hat{S}_A \cdot \hat{S}_B \rangle^{\mathrm{UHF}}_{A\neq B} = -\frac{3}{8} B_{AB} + m_A m_B + \frac{1}{2} \sum_{\mu\in A}\sum_{\nu\in B} |\rho^S_{\mu\nu}|^2, \tag{35}$$

which can be compared to Eq. (31) above.

Equations (29) and (30) were straightforward to implement in the ZINDO program because they utilize quantities already computed and stored by the program. A wrapper subroutine was added that successively executes the program for a list of input files and computes $\langle \hat{S}_A \cdot \hat{S}_B \rangle$ and B_{AB} for all unique combinations of A and B for each molecule. This proved convenient for the calculation of the coupling constants for polynuclear complexes, which requires a separate UHF calculation for each coupling constant in Eq. (1). This is considered in more detail below. The new subroutine also makes the appropriate sums to determine $\langle \hat{S}^2 \rangle$ according to Eq. (12) for each input file, which serves as a check and indicates the extent of spin contamination for UHF wave functions. The next section considers the connection between the Heisenberg coupling constants that describe the true spin states of the molecule and energies and local spin expectation values computed for spin-contaminated single determinant wave functions.

3. Connection Between Single Determinant Wave Functions and the Heisenberg Spin Model

In this section we consider how the local spin formulation might be used to extract coupling constants from RHF and UHF wave functions. The energy calculated from these wave functions contains terms aside from the energy of spin couplings (kinetic energies of electrons, electron–nuclear attraction, etc.). A zeroth-order energy must therefore be included in the usual expression of the HSM,

$$E^S = E_0 - \sum_{A<B} J_{AB}\langle S_A \cdot S_B\rangle^{(S)}. \quad (36)$$

Here, the superscript S indicates a particular value of the total spin quantum number. As with the traditional Heisenberg energy expression, it is assumed that this equation applies to spin eigenstates of the system obtained from coupling of high-spin radical centers. It is demonstrated here that in favorable cases good approximations of the coupling constants describing these spin states can be extracted from wave functions that are not spin eigenfunctions. This is true as long as both energies and local spin expectation values are taken from the approximate wave functions. This method is similar to the spin projection approach used by Noodleman and others [24–26] but general and avoids making approximations regarding the local spins. A formal proof is given and the new approach is illustrated by the example of two widely separated radical centers, each with two electrons.

It is well known that UHF wave functions are eigenfunctions of the z component of spin, $\hat{S}_Z$, but not of the total spin (excepting the case of all open-shell electrons high spin in a number of orbitals equal to the number of electrons) [19]. A UHF wave function with a particular value of S_z always has a value of $\langle S^2\rangle$ equal to or greater than $S_z(S_z + 1)$, and is thus said to be "contaminated" by contributions from spin eigenfunctions with $S > S_z$. Löwdin first demonstrated that an approximate, spin-contaminated wave function is equal to a weighted sum of wave functions that are eigenfunctions of total spin,

$$|^{\mathrm{UHF}}\Psi^{S_z}\rangle = \sum_{S\geq S_z} C_S|\Psi^S\rangle. \quad (37)$$

The wave functions $|\Psi^S\rangle$ are eigenfunctions of $\hat{S}^2$ and form an orthonormal set. This implies that

$$\sum_{S\geq S_z} |C_S|^2 = 1 \quad (38)$$

because the UHF wave function of Eq. (37) is normalized. Given Eqs. (37) and (38), both the UHF energy and total spin reduce to weighted sums over energies and expectation values of $\hat{S}^2$, respectively:

$$E^{\mathrm{UHF}} = \sum_{S\geq S_z} C_S^2 E^S \quad (39)$$

$$\langle {}^{\mathrm{UHF}}\Psi|\hat{S}^2|{}^{\mathrm{UHF}}\Psi\rangle = \sum_{S\geq S_z} C_S^2\langle\Psi^S|\hat{S}^2|\Psi^S\rangle = \sum_{S\geq S_z} C_S^2 S(S+1). \quad (40)$$

In the same way, the local spin expectation values $\langle\hat{S}_A \cdot \hat{S}_B\rangle$ for a UHF wave function display this spin contamination. Given Eq. (13),

$$\langle {}^{\mathrm{UHF}}\Psi|\hat{S}_A \cdot \hat{S}_B|{}^{\mathrm{UHF}}\Psi\rangle = \sum_{S\geq S_z} C_S^2\langle\Psi^S|\hat{S}_A \cdot \hat{S}_B|\Psi^S\rangle. \quad (41)$$

This result is intuitively clear because the expectation value of total spin is equal to the sum of $\langle\hat{S}_A \cdot \hat{S}_B\rangle$ over all A and B [Eq. (12)].

The HSM is assumed to correctly predict the relative energies of all spin states obtained from coupling of the radical centers in their high-spin states. For all but the simplest cases, these states represent only some of the possible spin states of the system. Other states can be obtained by coupling of radical centers that are not locally high spin. In the case of two radical centers each with two electrons, for example, states with $S = 0$, 1, and 2 are obtained if both centers are high spin. In addition, there are two triplet states obtained from coupling one atom locally in a singlet state with the other locally in a triplet state. There is also a singlet state obtained when both atoms are locally in singlet states. For a single determinant with $S_Z = 0$, the summation of Eq. (37) potentially runs over all six of these states. Because only three of them are described by the HSM, it is important to consider which spin functions contribute to a single determinant wave function if a connection between single determinants and the HSM is to be established. The following development shows that, in general, if a single determinant is an eigenfunction of the local spin operators $\{\hat{S}_A^2\}$ then the spin states contributing to the summation of Eq. (37) are also and have the same eigenvalues.

The spin projection technique originally formulated by Löwdin [27–29] allows the spin states and coefficients in Eq. (37) to be projected out of a single determinant wave function. The "Löwdin annihilator" is used to remove other spin functions from the summation. This operator is

$$\hat{A}_i^S = \frac{\hat{S}^2 - t(t+1)}{S(S+1) - t(t+1)}, \quad (42)$$

where t is the spin to be annihilated. Contributions of each spin state to the UHF wave function are fond by applying the Löwdin projector,

$$\hat{O}_S = \prod_{t \neq S} \hat{A}_t^S, \tag{43}$$

for that spin to the single determinant. Thus, the spin states of Eq. (37) are found by application of powers of the $\hat{S}^2$ operator to the single determinant. The $\hat{S}^2$ operator commutes with the local spin operators $\{\hat{S}_A^2\}$, so if the determinant is an eigenfunction of these operators repeated application of $\hat{S}^2$ will not change the local spin quantum numbers. Thus, if the local spin quantum numbers describing a single determinant wave function are high spin the UHF wave function is a linear combination of spin states described by the HSM. The conditions under which this is true are discussed below.

Given that the spin states contributing to Eq. (37) include only states described by the HSM, the energy expression of Eq. (36) can be substituted into the summation on the right side of Eq. (39). Doing so gives

$$E^{\mathrm{UHF}} = \sum_{S \geq S_z} C_S^2 \cdot \left(E_0 - \sum_{A<B} J_{AB} \langle S_A \cdot S_B \rangle^{(S)} \right) \tag{44}$$

or

$$E^{\mathrm{UHF}} = E_0 \sum_{S \geq S_z} C_S^2 + \sum_{S \geq S_z} C_S^2 \cdot \left(- \sum_{A<B} J_{AB} \langle S_A \cdot S_B \rangle^{(S)} \right). \tag{45}$$

Recalling Eq. (38) and rearranging the order of the summations in the second term on the right side of Eq. (45) yields

$$E^{\mathrm{UHF}} = E_0 - \sum_{A<B} J_{AB} \left(\sum_{S \geq S_z} C_S^2 \cdot \langle \hat{S}_A \cdot \hat{S}_B \rangle^{(S)} \right). \tag{46}$$

The summation in parentheses is identical to the right side of Eq. (41), giving

$$E^{\mathrm{UHF}} = E_0 - \sum_{A<B} J_{AB} \langle \hat{S}_A \cdot \hat{S}_B \rangle^{\mathrm{UHF}}. \tag{47}$$

This result is significant. It means that the same values of the coupling constants that describe the spin states of the system also describe any single determinant broken spin symmetry wave function, regardless of the extent of spin contamination, as long as that wave function is an eigenfunction of the local spin operators. Both the energy and the local spin expectation values must be taken for the broken spin wave function for Eq. (47) to be true. This is intuitively obvious, given Eqs. (37) and (41) above.

The results presented above are illustrated by two isolated atoms (or ions), each with two unpaired electrons. This is the simplest case in which both radical centers can take on different local spins. There are six spin states for this system, as each atom can be locally in a triplet state ($S_A = 1$) or a singlet state ($S_A = 0$). According to the proof give above, the single determinant wave functions $|\alpha\alpha\beta\beta\rangle$ and $|\beta\beta\alpha\alpha\rangle$, which are eigenfunctions of the local spin operators $\hat{S}_A^2$ and $\hat{S}_B^2$ (with eigenvalues of two in each case) but not of the total spin operator $\hat{S}^2$, are given by linear combinations of spin states described by the HSM that arise from coupling of two triplet atoms.

Wave functions for the six spin states are as follows. The total spin quantum number is given as a left superscript and the total z-component of spin is given as a right subscript in these equations. The electron spins are indicated by α for spin-up and β for spin-down, and it is assumed that the first two electrons are on the atom labeled A and the second two are on the atom labeled B.

$$\begin{aligned}
|^2\Psi_0\rangle &= \frac{1}{\sqrt{6}} [\alpha\alpha\beta\beta + \beta\beta\alpha\alpha + \alpha\beta\alpha\beta + \alpha\beta\beta\alpha + \beta\alpha\alpha\beta + \beta\alpha\beta\alpha] \\
|^1\Psi_0\rangle &= \frac{1}{\sqrt{2}} [\alpha\alpha\beta\beta - \beta\beta\alpha\alpha] \\
|^1\Psi_0\rangle' &= \frac{1}{2} [\alpha\beta\alpha\beta - \alpha\beta\beta\alpha + \beta\alpha\alpha\beta - \beta\alpha\beta\alpha] \\
|^1\Psi_0\rangle'' &= \frac{1}{2} [\alpha\beta\alpha\beta + \alpha\beta\beta\alpha - \beta\alpha\alpha\beta - \beta\alpha\beta\alpha] \\
|^0\Psi_0\rangle &= \frac{1}{\sqrt{12}} [2\alpha\alpha\beta\beta + 2\beta\beta\alpha\alpha - \alpha\beta\alpha\beta - \alpha\beta\beta\alpha - \beta\alpha\alpha\beta - \beta\alpha\beta\alpha] \\
|^0\Psi_0\rangle' &= \frac{1}{2} [\alpha\beta\alpha\beta - \alpha\beta\beta\alpha - \beta\alpha\alpha\beta + \beta\alpha\beta\alpha].
\end{aligned} \tag{48}$$

The origin of each of these six wave functions in terms of the local spins of each atom is made clear by expressing Eq. (48) in terms of local spin eigenfunctions,

$$|11\rangle^{\gamma} = \alpha\alpha$$

$$|10\rangle^{\gamma} = \frac{1}{\sqrt{2}}(\alpha\beta + \beta\alpha)$$

$$|1-1\rangle^{\gamma} = \beta\beta$$

$$|00\rangle^{\gamma} = \frac{1}{\sqrt{2}}(\alpha\beta - \beta\alpha), \tag{49}$$

where γ refers to the radical center, either A or B. Doing so gives

$$|^2\Psi_0\rangle = \frac{1}{\sqrt{6}}[|11\rangle^A|1-1\rangle^B + |1-1\rangle^A|11\rangle^B + 2|10\rangle^A|10\rangle^B]$$

$$|^1\Psi_0\rangle = \frac{1}{\sqrt{2}}[|11\rangle^A|1-1\rangle^B - |1-1\rangle^A|11\rangle^B]$$

$$|^0\Psi_0\rangle = \frac{1}{\sqrt{3}}[|11\rangle^A|1-1\rangle^B + |1-1\rangle^A|11\rangle^B - |10\rangle^A|10\rangle^B]$$

$$|^1\Psi_0\rangle' = |10\rangle^A|00\rangle^B$$

$$|^1\Psi_0\rangle'' = |00\rangle^A|10\rangle^B$$

$$|^0\Psi_0\rangle' = |00\rangle^A|00\rangle^B. \tag{50}$$

When expressed in this way, it is easily seen that the first three of these wave functions are obtained from coupling of two triplet atoms.

Application of the Löwdin projector $\hat{O}_S$ [Eq. (43)] to the broken spin single determinant $|\alpha\alpha\beta\beta\rangle$ for $S = 0$, 1, and 2 yields

$$|\alpha\alpha\beta\beta\rangle = \sqrt{\frac{2}{6}}|^0\Psi_0\rangle + \sqrt{\frac{3}{6}}|^1\Psi_0\rangle + \sqrt{\frac{1}{6}}|^2\Psi_0\rangle. \tag{51}$$

Thus, it is true that the spin states included in the sum of Eq. (37) for the single determinant wave function $|\alpha\alpha\beta\beta\rangle$ are limited to those described by the HSM. It is interesting to note that this single determinant, which might ostensibly be considered to be the UHF approximation of the singlet state, is 50% triplet. From Eq. (40), $\langle\hat{S}^2\rangle$ for this single determinant is equal to two, and because $\langle\hat{S}_A^2\rangle = \langle\hat{S}_B^2\rangle = 2$, $\langle\hat{S}_A \cdot \hat{S}_B\rangle = -1$.

Turning now to the exchange constant J_{AB} for this system, we proceed by substituting energies and local spin expectation values into Eq. (36) and solving simultaneously for E_0 and J_{AB}. Local spin expectation values and energies [assuming A and B are the same element (and charge) and have identical orbital occupancies] for $|^2\Psi_0\rangle$, $|^0\Psi_0\rangle$, and $|^{B.S.}\Psi_0\rangle = |\alpha\alpha\beta\beta\rangle$ are

$$^2E = 2\Gamma_{AA} + 4\Gamma_{AB} - 2K_{AA} - 4K_{AB} \quad \langle\hat{S}_A \cdot \hat{S}_B\rangle^{(2)} = 1$$

$$^0E = 2\Gamma_{AA} + 4\Gamma_{AB} - K_{AA} + 2K_{AB} \quad \langle\hat{S}_A \cdot \hat{S}_B\rangle^{(0)} = -2$$

$$^{B.S.}E = 2\Gamma_{AA} + 4\Gamma_{AB} - 2K_{AA}$$

$$\langle\hat{S}_A \cdot \hat{S}_B\rangle^{(B.S.)} = -1, \tag{52}$$

where Γ_{AB} is a Coulomb repulsion integral for repulsion of electrons on centers A and B (this notation is adopted to avoid confusion with the Heisenberg coupling constant J_{AB}) and K_{AB} is an exchange integral. Substituting these quantities for $|^2\Psi_0\rangle$ and $|^0\Psi_0\rangle$ into Eq. (36) and solving simultaneously yields $E_0 = 2\Gamma_{AA} + 4\Gamma_{AB} - 2K_{AA} - 2K_{AB}$ and $J_{AB} = 2K_{AB}$. If instead we consider $|^2\Psi_0\rangle$ and $|^{B.S.}\Psi_0\rangle$, and replace ^0E with $^{B.S.}E$ and $\langle\hat{S}_A \cdot \hat{S}_B\rangle^{(0)}$ with $\langle\hat{S}_A \cdot \hat{S}_B\rangle^{(B.S.)}$ in Eq. (36), solving simultaneously gives the same values for E_0 and J_{AB}. In other words, the same value of J_{AB} is obtained using $|^0\Psi_0\rangle$ or $|^{B.S.}\Psi_0\rangle$. In this example it is straightforward to use either $|^0\Psi_0\rangle$ or $|^{B.S.}\Psi_0\rangle$, but in more complicated cases like the hexanuclear iron complexes considered below, with 30 open-shell electrons, it is possible to obtain broken-spin single determinant wave functions with a semiempirical method like INDO/S, but impossible to obtain variational wave functions for the true spin states because of their intractably large number.

The primary assumption made in the preceding discussion was that the single determinant wave

function is an eigenfunction of the local spin operators. Several requirements must be met for this to be the case. The open-shell orbitals must be local to the magnetic centers and all open-shell orbitals must be singly occupied. All open-shell electrons on a given radical center must have the same spin, although spins on different radical centers might be reversed relative to each other. Also, if there are ligands present α and β orbitals containing ligand electrons must occur in identical pairs, as they would in a closed-shell Slater determinant for the isolated ligand. This is in general not the case for UHF wave functions with any unpaired α spins, which have different orbitals for different spins due to spin polarization. We refer to a determinant that has the above-mentioned properties as an orbitally restricted Slater determinant (ORSD). The expectation value of the $\hat{S}^2$ operator for an ORSD is given by

$$\langle \hat{S}^2 \rangle^{\mathrm{ORSD}} = S_z^2 + S_{\max}, \tag{53}$$

where $S_{\max}$ is the maximum spin that would be obtained if all unpaired electrons had α spin. In the case of an ORSD wave function of a diferric complex, for example, $S_{\max}$ is equal to five because Fe^{+3} ions each have five unpaired electrons. Thus, the expectation value $\langle \hat{S}^2 \rangle^{\mathrm{ORSD}}$ is equal to five for the ORSD with $S_z = 0$. The import of Eq. (47) is that if the UHF wave function was an ORSD then the same coupling constants that describe the true spin states of the system also describe the ORSD.

This situation will rarely if ever be encountered outside of hypothetical test cases. In a transition metal complex the metal orbitals will typically mix at least somewhat with the ligand orbitals, and the ligand orbitals will not form a restricted set due to spin polarization. The deviation of a UHF single determinant from the conditions required of an ORSD can be seen by comparing $\langle \hat{S}^2 \rangle^{\mathrm{UHF}}$ with the right side of Eq. (53). Because there will in general be some deviation, the equivalence between coupling constants extracted from UHF wave functions and those describing the actual spin states of the system is thus only approximately true, even when all open-shell orbitals are (approximately) local, all are singly occupied, and all electrons on each metal are of the same spin. It is our experience that when these conditions are met UHF wave functions are approximately eigenfunctions of the local spin operators (as judged by expectation values of these operators). This is demonstrated below for the 10 complexes discussed in this article. In such cases we expect that coupling constants extracted from the UHF wave functions are good approximations of the true coupling constants.

It must be emphasized that all of the electrons on each metal must be of the same spin for accurate coupling constants to be obtained. This is vividly illustrated by the previous INDO/S calculations on the complex $[Fe_2S_2(SH)_4]^{-2}$ [4]. Anticipating results presented below, wave functions for the $S_z = 5$ and $S_z = 0$ components have expectation values $\langle \hat{S}^2 \rangle^{\mathrm{UHF}}$ close to those expected for ORSDs. These components are thus approximately eigenfunctions of the local spin operators, with expectation values close to the value of 8.75 expected for $S_A = 5/2$ Fe^{+3} ions. The coupling constant obtained using the energies of these components was -98 cm^{-1} [4], in reasonable agreement with known values for similar complexes ranging from -54 to -183 cm^{-1} [30, 31]. The $S_z = 4$ component, on the other hand, is not even approximately an eigenfunction of the local spin operators because the spin of one 3*d* electron on one of the metals must be flipped relative to the others to obtain $S_z = 4$. Using this component together with the $S_z = 5$ component to obtain an estimate of the exchange constant gave a grossly inaccurate value of $+913$ cm^{-1}. It is crucial to use only components in which all electrons on each metal have the same spin if accurate estimates of the exchange constants are to be obtained.

It should be noted that only metal ions with five or fewer *d* electrons can meet this requirement. We leave consideration of metals with greater than half-filled *d* orbitals for possible future work because the Fe^{+3} ions in the present set of complexes are high-spin d^5. As the results described below show, exchange constants obtained for these complexes with UHF energies and local spin expectation values compare well with constants obtained from fitting to variable-temperature magnetic susceptibility data.

4. Method for Obtaining Coupling Constants and Spin States of Polynuclear Transition Metal Complexes

In this section we consider how the coupling constants $\{J_{AB}\}$ for a polynuclear transition metal complex might be determined using single determinant wave function calculations. In doing so we

assume that all of the metals (and only the metals) in a complex have radical character. Hence, the only nonzero exchange constants will be between metals, although some of these may be zero as well. These assumptions, which are standard in virtually all inorganic applications of the HSM, limit the summations over A and B in Eq. (47) to run over the metals only. A complex with N_m metals has $1/2\,N_m(N_m - 1)$ exchange constants, plus the spin-independent term E_0. There are thus $1/2\,N_m(N_m - 1) + 1$ parameters to be determined. For a particular UHF component, E^{UHF} and the spin couplings $\langle S_A \cdot S_B\rangle^{\mathrm{UHF}}$ between metal centers also number $1/2\,N_m(N_m - 1) + 1$. If these quantities were computed for this same number of unique UHF wave functions, then Eq. (47) provides a system of $1/2\,N_m(N_m - 1) + 1$ equations linear in $1/2\,N_m(N_m - 1) + 1$ unknowns. These equations could be solved simultaneously for E_0 and the coupling constants. This is the approach we adopt.

Consider, for the sake of discussion, an unrestricted single determinant molecular orbital wave function as described in the previous section: All metal d orbitals remain local and are singly occupied. Further, assume that all of the unpaired electrons in the complex are spin-up. We refer to such a wave function as "high spin." If this high-spin wave function was obtained from a self-consistent field (SCF) calculation, it might be possible to reverse the spins of all of the electrons local to a particular metal ion, then reconverge the orbitals to self-consistency while maintaining their local aspect. In this way it might be possible to obtain a number of single determinant wave functions by successively "flipping the spins" of the various metals in different ways. These determinants would approximately meet the requirements of the previous section, and could therefore provide good estimates of the coupling constants of the complex.

Nominally, there are 2^{N_m} different ways of flipping the spins, although half must be discarded because they are simply the reverse of the others and yield no unique information. In the case of two metals, for example, "up–up" and "down–down" (where "up" and "down" refer to the direction of the z-component of spin of each metal) have the same Hamiltonian of Eq. (46), including sign and value of the coupling constant. "Up–down" and "down–up" likewise also have the same HSH. Thus, there are 2^{N_m-1} unique wave functions defined by flipping the spins, which is always equal to or greater than $1/2\,N_m(N_m - 1) + 1$, the number of exchange constants plus E_0. In complexes containing five or more metals, the high-spin wave function plus all wave functions obtained by flipping two spins provides a set of $1/2\,N_m(N_m - 1) + 1$ unique wave functions. Computing the energy and local spin expectation values $\{\langle S_A \cdot S_B\rangle^{\mathrm{UHF}}\}$ for each of these provides all the necessary data for obtaining the coupling constants $\{J_{AB}\}$.

Up to this point, single determinant wave functions defined by "flips" of the z-component of spin of electrons in local metal d orbitals have been referred to in an abstract sense. In practice, it can be difficult to obtain such wave functions due to SCF convergence problems and because of the inherently delocalized nature of MO wave functions. We found a procedure that consistently works to overcome these problems. The details are give later in the section describing computational implementation. The resulting local orbitals are used as a starting guess for UHF calculations, with d orbitals of each metal put in the α or β orbital manifolds as necessary to achieve the spin flips.

Converged UHF orbitals obtained in this way do not in general resemble the conceptual picture invoked above, with all of the metal d orbital character confined to a distinct set of orbitals. The d orbital character is instead dispersed throughout the orbital manifold, and can be identified only through properties such as the spin density [which is directly related to the local z-component of spin, Eq. (35)] and local spin expectation values. These properties display the behavior expected for open-shell metal complexes, with virtually all of the nonzero spin density in the metal d orbitals, and large local spin expectation values $\langle S_A \cdot S_A\rangle$ obtained for the metals that are similar to values expected for eigenfunctions of the local spin operators. These properties will be illustrated and discussed later. We are at present considering transformations of the UHF wave functions to provide a more conceptual set of orbitals.

Another point to consider is that for complexes with more than three metals there are always more ways to flip sins than parameters in the Heisenberg model. In the case of 6 metals, for example, there are 32 unique ways of flipping spins, while only 16 wave functions are needed to obtain the 15 coupling constants and E_0. The implication of Eq. (47) is that as far as the HSM is correct in assuming a universal set of coupling constants for the spin states it describes these same constants describe the energies of all single determinant wave functions of the type discussed above. If this is true, then the same values should be obtained for the coupling

constants regardless of which set of 16 wave functions are chosen out of the 32 possibilities. This has not in general been observed in previous theoretical treatments (see, e.g., Ref. [4]), where it has been found that the values obtained for coupling constants depend on the particular choice of components used. These approaches have not had the internal consistency that ours has, however, because idealized values of the local spin quantum numbers were used. We have not yet examined this systematically but found by trial and error with the larger complexes discussed below that estimates of coupling constants have little dependence on exactly which components are used. This hypothesis could be investigated by using a least-squares fitting procedure to obtain coupling constants from an excess number of UHF components. This would directly provide an estimate of the error incurred by selecting a certain subset of components. We are at present investigating this with several of the complexes discussed in this article.

Once the coupling constants have been obtained as described above, they can be substituted into the HSH, Eq. (1). Diagonalization of the operator of Eq. (5) then yields the energies and compositions of the true spin states of the system. In this way it is possible to predict the spin ground state of a polynuclear transition metal complex without resorting to expensive spin-adapted methods. The states obtained from the HSH can also be used to predict properties, such as the z component of spin for each metal. This is obtained in a straightforward way for spin states of the form of Eq. (6). It would also be feasible to obtain a theoretical estimate of variable-temperature magnetic susceptibility curves using the spin-state energies.

5. Computational Implementation: ZILSH

The local spin formalism has been implemented in the ZINDO program [6] and can be used with either RHF or UHF wave functions computed with the semiempirical methods INDO/S [7, 9, 15, 16], INDO/1 [7, 8, 16], AM1 [32], MNDO [33, 34], PM3 [35, 36], NDDO-G [37], CNDO [38, 39], INDO [40], PPP [41–44], and extended Hückel [45–51]. A wrapper subroutine was added to ZINDO that successively executes the program and computes local spin expectation values for a list of input files. This is convenient for calculations of Heisenberg coupling constants as described above, in which a number of calculations for the different spin flips must be run. All of the calculations described in this article used the INDO/S model (intermediate neglect of differential overlap model parameterized for optical spectroscopy), which is known to provide reasonable approximations of the energies of ground and excited states of open-shell transition metal complexes [4, 8–11, 15, 16, 52–60], in particular those of Fe^{+3} [4, 9, 52, 60]. The values used for all parameters in the model were those originally suggested by Zerner et al. [9].

The first step in solving for the coupling constants is to obtain local orbitals to serve as a starting guess for the various UHF calculations. At this initial stage, severe SCF convergence problems are often encountered. SCF convergence is not straightforward for polynuclear transition metal complexes for several reasons. First, initial guess wave functions are typically delocalized, which often is not a realistic assumption for the metal d orbitals that tend to retain atomic character. Second, when the spin coupling between metals is weak there are often many configurations of the metal d electrons with similar energies, so oscillation between two or more of these configurations can occur from cycle to cycle during the SCF process. Third, the energy gap between the d orbitals and both the occupied orbitals and the virtual (unoccupied) orbitals is often small, which can again lead to oscillation.

An approach that is successful in overcoming the problems listed above is as follows. To counter the problem of oscillation between different configurations, the configuration-averaged HF (CAHF) method [61] is used. This method is a modification of the ROHF formalism and uses a Fock operator constructed assuming an average over all possible configurations within a fixed active space. This neatly avoids the problem of oscillation. The active space includes all d orbitals and d electrons in the calculations reported here. It is also often necessary to use a level shift in these calculations to counter the problem of small energy gaps between closed- and open-shell orbitals and between open-shell and virtual orbitals. On the first cycle of the SCF procedure, the energy of the open-shell orbitals is shifted to higher energy by an atomic unit (a.u.), and the virtual orbitals are shifted above the open-shell orbitals by an a.u. On each of the next nine cycles, the shift is reduced to one divided by the iteration number, in a.u. In this way the level shift is half an a.u. on the second cycle, a third of an a.u. on the third cycle, and so on. The level shift is then discontinued after the 10th cycle. In some cases, the

difference in SCF energy on successive cycles would oscillate up and down by as much as an a.u. without this level shift procedure, but regular SCF convergence is quickly obtained in all cases with the level shift.

The CAHF orbitals obtained as just described are then used as a starting guess for ROHF calculations assuming high spin. In this step, the open shell is comprised of delocalized combinations of the metal *d* orbitals. Typically, no level shift is necessary; in all cases considered here, these calculations converged rapidly. Next, the open-shell orbitals are localized using the Boys procedure [62–65]. The ZINDO program was altered so that only the open-shell orbitals are transformed in this step. This avoids applying the lengthy Boys procedure to the closed-shell and virtual orbitals, which are numerous for the larger complexes considered here. In the case of $Fe_6O_2(OH)_2(OAc)_{10}(C_{10}H_{13}N_4O)_2$, for example, there are 216 closed-shell orbitals and only 30 open-shell orbitals.

The next step is to perform UHF calculations using the orbitals obtained in the previous step as a starting guess. Up to this point, the calculations are best carried out interactively. In this step it is impractical to do so, however, because 16 separate UHF calculations must be run for the hexanuclear complexes. We also anticipate applying the new approach to larger complexes, such as the SMMs $[Fe_8O_2(OH)_{12}(tacn)_6]^{+8}$ [66–68] and $[Mn_{12}O_{12}(O2CCH_3)_{16}(H_2O)_4]$ [69–75]. In the latter case, 67 calculations are required. Some degree of automation is thus important. A program was written that reads the ROHF-localized open-shell orbitals, constructs the somewhat lengthy input needed to assign orbitals on each metal to the α or β orbital manifold as necessary to obtain the various spin flips, and builds input files for the UHF calculations. Then, the wrapper subroutine described above is used to run the calculations. Another program then extracts the energies and local spin expectation values from the UHF output files, builds the set of simultaneous equations, and solves for the values of E_0 and the coupling constants. The equations are solved using standard linear algebra techniques [76].

Given values of the coupling constants, the HSH of Eq. (5) is expanded in the basis of the $\{|S_A S_{zA}\rangle|S_B S_{zB}\rangle\cdots\}$ and the resulting matrix diagonalized to obtain the final spin-state energies and wave functions. The expectation value of the operator $\hat{S}_{zA}$ for the metals is computed for each state. In all cases considered here, direct diagonalization of the entire matrix was performed using a standard linear algebra subroutine [77]. The largest basis considered included 4332 spin states that result from the coupling of six $S_A = 5/2$ metals. Larger complexes will be more difficult to treat. A complex with eight $S_A = 5/2$ metals, for example, would have a basis of over 130,000 spin states. In such cases recourse to sparse matrix techniques that approximate a few of the lowest roots of the HSH matrix will be necessary.

In summary, the methodology for obtaining coupling constants and spin-state energies and wave functions is as follows: Starting orbitals are obtained using the CAHF method with level shift for the high-spin case. The resulting orbitals are used as the starting point for obtaining an ROHF wave function for the high-spin case. The open-shell ROHF orbitals are then localized using the Boys procedure. The local orbitals are used as the starting guess for UHF calculations in which electrons on the various metals are assigned to the α or β manifolds to obtain spin flips. Energies and local spin expectation values from the UHF calculations are substituted into Eq. (46), and the resulting set of equations solved to yield the coupling constants. Finally, the coupling constants are substituted into the HSH, Eq. (1), to yield the final spin states and their energies. We refer to this method as ZILSH, derived from ZINDO, Davidson's local spin formalism, and the Heisenberg spin model.

6. Test Cases

Ten polynuclear iron complexes are discussed in this article (Table I). The number of metals per complex ranges from two to six, and all metals are high-spin Fe^{+3} ions. The complexes are relevant to molecular magnetism and biochemistry and were chosen to test the theoretical procedure described herein. The choices were also designed to test approximations typically made in fitting coupling constants to reproduce magnetization vs. temperature data. All molecular structures except that of $[Fe_2S_2(SH)_4]^{-2}$ were taken from either the Cambridge Structural Database or the Indiana University Molecular Structure Center. Counterions and resolved solvent molecules, if any, were omitted and estimated hydrogen atom positions were used when available. In cases where hydrogen atoms were not included in a structure (usually just a few hydrogen atoms were omitted), they were added to the structure and their positions minimized using

TABLE I
Complexes used as test cases.

Complex	Spin of ground state
$[Fe_2S_2(SH)_4]^{-2}$	0
$[(HB(pz)_3Fe)_2O(OAc)_2]$	0
$[(HB(pz)_3Fe)_2(OH)(OAc)_2]^{+}$	0
$[Fe_3O(TIEO)_2(O_2CPh)_2Cl_3]$	5/2
$[Fe_4O_2(OAc)_7(bpy)_2]^{+}$	0
$[Fe_4O_2Cl_2(OAc)_6(bpy)_2]$	0
$[Fe_4(OCH_3)_6(dpm)_6]$	5
$[Fe_6O_2(hmp)_8Cl_4]^{+2}$	0
$[Fe_6O_2(OH)_2(OAc)_{10}(C_{10}H_{13}N_4O)_2]$	5
$[Fe_6O_3(OAc)_9(OEt)_2(bpy)_2]^{+}$	0

Ground-state spins determined based on experimental magnetization experiments. See text for descriptions, nomenclature, and references. Schematic diagrams of the metal frameworks of complexes with three or more metals are shown in Figures 1–7.

the MM+ force field implemented in the Hyperchem program [78] while holding the rest of the structure fixed. The structure of $[Fe_2S_2(SH)_4]^{-2}$, which is a hypothetical complex designed to model ferrodoxins, was taken from Ref. [4]. A short description of each complex is given below.

6.1. $[Fe_2S_2(SH)_4]^{-2}$

This hypothetical complex is a model of the ferrodoxins, a class of iron–sulfur proteins involved in transport and storage of electrons in many enzymes [30, 79]. Ferrodoxins make up the active site and associated electron transfer systems in nitrogenase, for example [80].

The coupling constant for interaction of the two iron atoms in this complex has not been determined based on experimental data. However, coupling constants known for a number of naturally occurring ferrodoxins and synthetic ferrodoxin analogs range from -54 to -183 wave numbers [30, 31]. The electronic structure and magnetic coupling in this complex were extensively studied using INDO/S ROHF, UHF, and projected UHF calculations [4]. These calculations did not use the local spin operator, and assumed that $S_A = S_B = 5/2$ in each case, despite the large spin contamination of the UHF wave functions. Here, we investigate this approximation and compare the previous work with the new approach for obtaining the coupling constant.

6.2. $[(HB(pz)_3Fe)_2O(OAc)_2]$ AND $[(HB(pz)_3Fe)_2(OH)(OAc)_2]^{+}$ [81]

These complexes were chosen because the only difference in their composition is protonation of the μ_2-oxide bridge in the former to yield the latter. OAc^{-} is the acetate anion, and $HB(pz)_3^{-}$ is the hydridotris(1-pyrazolyl)borate anion. Protonation of the bridging oxide has a large effect on the coupling constant found from experiment, reducing it from -121 cm^{-1} in the first complex to -17 cm^{-1} in the second complex [81]. The Fe-(μ_2-O) distance also changes from 1.784 to 1.956 Å as a result of the protonation. The coupling constant in dinuclear oxide-bridged iron complexes typically ranges from -100 to -150 cm^{-1} but is in general known to be reduced by protonation [82]. As shown below, the INDO/S parameters and the new method of determining coupling constants is apparently able to account for the effect of protonation of an oxide bridge.

6.3. $[Fe_3O(TIEO)_2(O_2CPh)_2Cl_3]$

In this complex the iron ions form a nearly isosceles triangle, bridged by a central μ_3-oxide ligand [83] (Fig. 1). $TIEO^{-}$ is the deprotonated anion of 1,1,2-tris(1-methylimidazole-2-yl)ethanol and serves as a tridentate ligand. The legs of the triangle are each bridged by the central oxide ligand, the alkoxide oxygen of $TIEO^{-}$, and a carboxylate ligand, and have Fe—Fe distances of roughly 3.02 Å. The base of the triangle is bridged only by the central oxide ligand, and has an iron–iron distance of 3.67 Å. The structure is somewhat unusual, as most triangular iron carboxylate complexes are equilateral [84]. Ex-

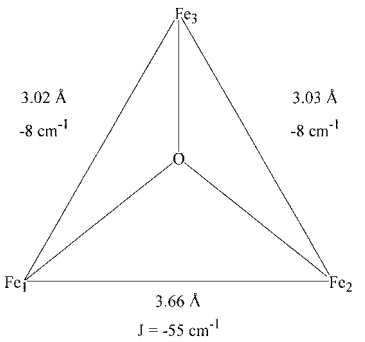

FIGURE 1. Structural framework of $[Fe_3O(TIEO)_2(O_2CPh)_2Cl_3]$, including Fe—Fe distances and coupling constants from fit to variable-temperature magnetic susceptibility data. See text for discussion and references.

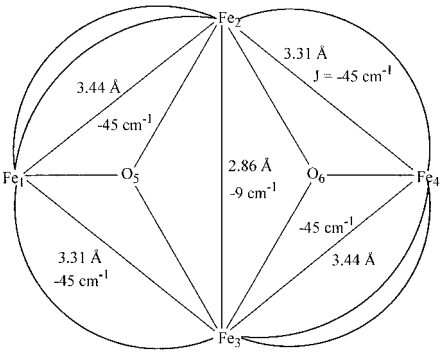

FIGURE 2. Structural framework of $[Fe_4O_2(OAc)_7(bpy)_2]^+$, including Fe—Fe distances and coupling constants from fit to variable-temperature magnetic susceptibility data. Curved lines represent carboxylate bridges. Fe_2 and Fe_3 are bridged by an additional carboxylate that is not shown. See text for discussion and references.

change constants (Fig. 1) were fit to reproduce variable-temperature magnetic susceptibility data. It can be inferred from these coupling constants that the complex has a ground state with $S = 5/2$, which is also consistent with the results of Mössbauer spectroscopy [83].

6.4. $[Fe_4O_2(OAc)_7(bpy)_2]^+$ [82]

This complex was prepared as a synthetic analog of iron-containing metalloproteins with bridging oxide and carboxylate ligands, such as ferritin (an iron storage protein) [85, 86], ribonucleotide reductase [87], and the hemosiderins [88–90]. Here, bpy is 2,2′-bipyridine. The complex has a $[Fe_4O_2]^{+8}$ "butterfly" core (Fig. 2) that has been observed for a number of tetranuclear iron [82, 91–94], manganese [95–103], chromium [104, 105], and vanadium [106] complexes. This topology has two "body" metals bridged by two μ_3-oxide ligands and two "wingtip" metals that each share a μ_3-O ligand with the body metals. It is typically assumed that the four exchange interactions between the wingtip and body ions (J_{wb}) are equivalent when fitting coupling constants to reproduce variable-temperature magnetic susceptibility data. In the case of $[Fe_4O_2(OAc)_7(bpy)_2]^+$ this is only approximate, based on both Fe—Fe distances and the number of bridges between metals, as shown in Figure 2. It is also assumed that the wingtip–wingtip interaction (J_{ww}) is zero. Under these assumptions the fit yielded values of $J_{wb} = -45.0\ cm^{-1}$ and $J_{bb} = -8.9\ cm^{-1}$. However, J_{bb} was found to be indeterminate from the fit, as values ranging from -15 to $+105\ cm^{-1}$ give the same relative error in the fit. This occurs because J_{wb} is much larger than J_{bb}, so the value of J_{bb} does not have any effect on states with energies less than 300 K. McCusker et al. thus concluded that J_{bb} is greater than $-15\ cm^{-1}$ and probably antiferromagnetic [82]. The calculations described here provide a more precise estimate of the value of J_{bb} for this complex.

It can be inferred from the above values of J_{bb} and J_{wb} that the ground state of this complex is diamagnetic ($S = 0$). It is interesting to note that the spin moments of the two body irons appear to be aligned ferromagnetically in this ground state, despite the intrinsically antiferromagnetic nature of this coupling. This occurs because of the much larger size of the J_{wb} interactions and is often referred to as "spin frustration" [82].

6.5. $[Fe_4O_2Cl_2(OAc)_6(bpy)_2]$ [107]

This complex has a $[Fe_4O_2]^{+8}$ butterfly core similar to that of the previous complex, except that the core is much less symmetrical in terms of both the Fe—Fe distances and the ligands of each metal (Fig. 3). Even so, it was assumed that all J_{wb} interactions were equal in fitting coupling constants to reproduce variable-temperature magnetic susceptibility data [107]. We wanted to investigate this approximation for such an asymmetrical core. Values obtained from the fit were $J_{bb} = -10.9\ cm^{-1}$ and $J_{wb} = -41.0\ cm^{-1}$, although again the value of J_{bb} was indeterminate, as described above.

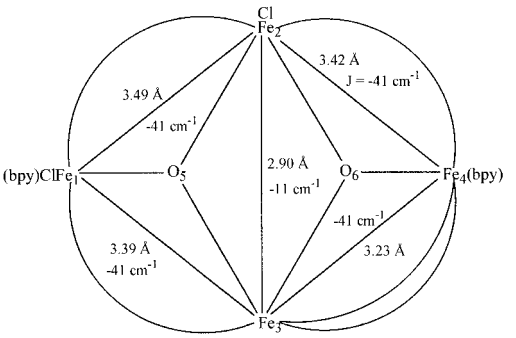

FIGURE 3. Structural framework of $[Fe_4O_2Cl_2(OAc)_6(bpy)_2]$, including ligands, Fe—Fe distances, and coupling constants from fit to variable-temperature magnetic susceptibility data. Curved lines represent carboxylate bridges. Fe_2 and Fe_3 are bridged by an additional carboxylate that is not shown. See text for discussion and referrences.

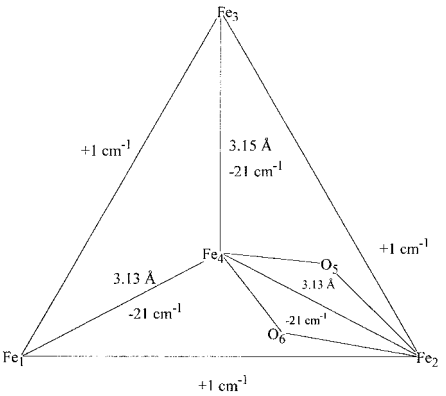

FIGURE 4. Structural framework of $[Fe_4(OCH_3)_6(dpm)_6]$, including Fe—Fe distances and coupling constants from fit to variable-temperature magnetic susceptibility data. O_5 and O_6 are part of OCH_3^- ligands. Other OCH_3^- ligands bridging apex iron ions and Fe_4 omitted for clarity. See text for discussion and references.

6.6. $[Fe_4(OCH_3)_6(dpm)_6]$ [108]

This complex functions as an SMM [108] and has a different topology than the two tetranuclear complexes just described. Three of the iron ions form a roughly equilateral triangle and are connected to a central metal via bridging ligands (Fig. 4). The ligand dpm^- is the deprotonated anion of dipivaloylmethane. A fit to variable temperature-magnetic susceptibility data yielded the exchange constants shown in Figure 4. The value of -21 cm^{-1} obtained for the apex–center couplings agrees well with an empirical model relating couplings in diiron complexes with the length of the shortest superexchange pathway [109] (a more recent article reports a dependence on Fe-(μ_2-O)-Fe angle as well as the Fe-(μ_2-O) distance for the same set of complexes [110]). The small, positive couplings found between apex irons (which are not directly bridged) are similar to next-nearest-neighbor interactions in chromium clusters [111]. The ground state of this complex has $S = 5$.

6.7. $[Fe_6O_2(hmp)_8Cl_4]^{+2}$ [84]

This and the next complex have structures with two $Fe_3(\mu_3$-O) units connected by bridging ligands (Fig. 5). The ligand hmp^- is hydroxymethylpyridine. In this complex the four central irons are approximately planar and the iron framework has a chair conformation. The complex has an inversion center. In fitting of coupling constants to reproduce variable-temperature magnetic susceptibility data, all couplings other than J_{12}, J_{13}, J_{23}, and J_{24} (using the numbering scheme of Fig. 5) and their symmetry-equivalent counterparts were assumed to be zero. It was also assumed that $J_{12} = J_{13}$ due to approximate symmetry. Values obtained from the fit were $J_{12} = J_{13} = -18$ cm^{-1}, $J_{23} = -52$ cm^{-1}, and $J_{24} = -3$ cm^{-1} [84], indicating that the ground state has $S = 0$. However, a variable-field magnetization experiment indicated that the spin of the ground state is three. Christmas et al. suggested that this could result from a thermal average over several states to give an effective spin of three [84]. This hypothesis is supported by the fact that states with $S = 1$, 2, 3, and 4 lie within 10 cm^{-1} of the $S = 0$ ground state, according to the HSM using the above values for the coupling constants.

6.8. $[Fe_6O_2(OH)_2(OAc)_{10}(C_{10}H_{13}N_4O)_2]$ [84, 112, 113]

This complex has a similar arrangement of six Fe^{+3} ions, except that the iron framework is much closer to planar and each triangular unit has a larger degree of asymmetry (Fig. 6; the complex as a whole still has inversion symmetry). The ligand $C_{10}H_{13}N_4O^-$ is the deprotonated anion of bis(2-*N*-methylimidazole-2-yl)-2-hydroxyethane. Despite the marked asymmetry of the core, it was assumed in

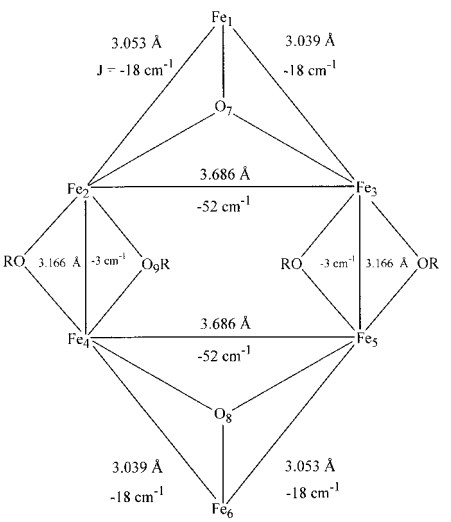

FIGURE 5. Structural framework of $[Fe_6O_2(hmp)_8Cl_4]^{+2}$, including Fe—Fe distances and coupling constants from fit to variable-temperature magnetic susceptibility data. OR represents hmp^- ($C_6H_6NO^-$). See text for discussion and references.

fitting coupling constants based on variable-temperature magnetic susceptibility data that $J_{13} = J_{23}$ (see Fig. 6 for numbering scheme) due to the similarity in bridging ligands [84]. J_{12} was allowed to take on a different value because this pathway is bridged by one μ_3-O ligand and one μ_2-alkoxide ligand, while the J_{13} and J_{23} pathways are bridged by only a μ_3-O ligand. As shown in Figure 6, the coupling constants obtained from the fit were $J_{13} = J_{23} = -38$ cm^{-1}, $J_{12} = -5.6$ cm^{-1}, and $J_{24} = -7.5$ cm^{-1}, from which a ground-state spin of 5 can be inferred.

6.9. $[Fe_6O_3(OAc)_9(OEt)_2(bpy)_2]^+$ [114]

This hexanuclear complex has a different topology than the previous two, with two $[Fe_3O]^{+7}$ scalene triangular units bridged by a central (μ_4-O) ligand (Fig. 7). The iron ions are not coplanar, with the plane defined by one Fe_3 unit tilted relative to the plane defined by the other Fe_3 unit. Variable-temperature magnetic susceptibility data indicate a ground state with $S = 0$. No attempt was made to fit coupling constants due to the complex nature of the couplings and lack of molecular symmetry. Seddon et al. predicted that the spins would align as shown in Figure 7 based on the expected antiferromagnetic coupling between high-spin Fe(III) ions and anticipated spin frustration effects in the complex [114].

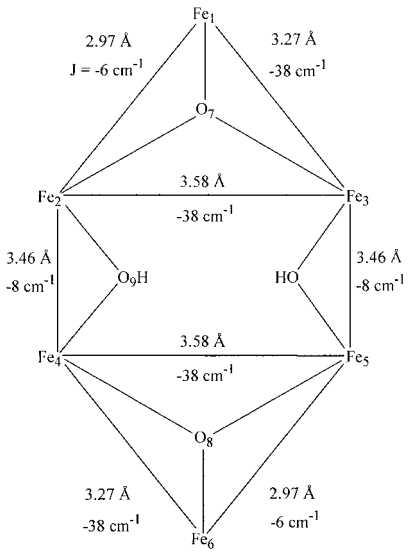

FIGURE 6. Structural framework of $[Fe_6O_2(OH)_2(OAc)_{10}(C_{10}H_{13}N_4O)_2]$, including Fe—Fe distances and coupling constants from fit to variable-temperature magnetic susceptibility data. See text for discussion and references.

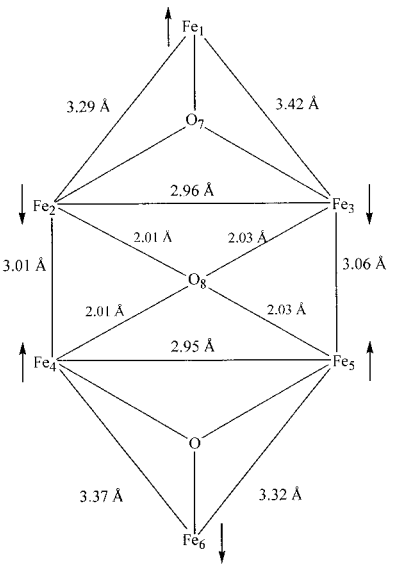

FIGURE 7. Structural framework of $[Fe_6O_3(OAc)_9(OEt)_2(bpy)_2]^+$, including selected Fe—Fe and Fe—O distances. See text for discussion and references.

7. Results and Discussion

Results obtained for each complex include energies of various UHF spin components and local spin expectation values $\langle \hat{S}_A \cdot \hat{S}_B \rangle$ for each component. It is also instructive to consider the local z-component of spin for each metal, m_A, defined as one half the sum of diagonal elements of the spin density matrix for all orbitals on that metal [Eq. (34)]. Also, the diagonal elements of the spin density matrix individually represent the spin density present in each atomic orbital. Together with the local z-components, this quantity indicates which atoms and orbitals have open-shell character in a UHF wave function. Heisenberg coupling constants have been computed for exchange interactions between the metals of each complex. Substitution of these values into the HSH [Eq. (1)] and diagonalization yielded energies of the spin states of the complex and their compositions in terms of the expansion coefficients of Eq. (6). Z-components of spin for each metal, $\langle \hat{S}_{zA} \rangle$, computed for the spin states indicate the distribution of open-shell electrons. Results

are grouped by complex in the following discussion.

7.1. $[Fe_2S_2(SH)_4]^{-2}$

Calculations on this model ferrodoxin following the method outlined above yielded the same $S_z = 0$ and $S_z = 5$ UHF components obtained previously [4], with the former 2940 cm^{-1} lower in energy than the latter. In both cases the unpaired spins reside almost exclusively on the iron ions, as indicated by the quantity $2m_A$ (Table II). Nominally, values of ± 5 would be expected for each iron and zero for each ligand atom, which is approximately demonstrated by the values obtained for both components. Deviations occur because of covalent interaction with the ligand orbitals and are typical of those found using *ab initio* single determinant wave functions of DFT densities. For example, recent DFT calculations on the complex $[Fe(OCH_3)_2(O_2CCH_2Cl)]_{10}$ yielded local z-componets of spin of 4.24 for each iron [115]. It is seen when considering the diagonal element of the spin density matrix for each orbital of the iron ions (Table III) that the unpaired spin on each metal largely resides in the 3d orbitals, as expected for high-spin Fe^{+3} ions. Together, the results of Tables II and III indicate that the $S_z = 5$ and $S_z = 0$ UHF components are reasonable approximations of eigenfunctions of the local spin operators with $S_A = 5/2$. This is supported by the expectation values $\langle \hat{S}_A^2 \rangle$ for the metals (Tables IV and V), which are close to the formal value of 8.75 in each case. Local z-components of spin are similar to those of Tables II and III for all other complexes considered and will not be discussed.

TABLE II

2 × local z-components of spin of the atoms of $[Fe_2S_2(SH)_4]^{-2}$ for the $S_z = 5$ and $S_z = 0$ components defined as the sum of diagonal elements $\rho^S_{\mu\mu}$ for all orbitals centered on the atom [Eq. (34)].

Atom	$S_z = 5$	$S_z = 0$
Fe_1	4.621	4.502
Fe_2	4.621	−4.502
$S(H)$	0.024	0.014
$H(S)$	0.003	0.003
μ_2-S	0.326	0.000
$S'(H)$	0.024	−0.014
$H(S')$	0.003	−0.003

TABLE III

Orbital spin densities for atomic orbitals of $Fe_{(2)}$ of $[Fe_2S_2(SH)_4]^{-2}$, $S_z = 5$ and $S_z = 0$ components, defined as the diagonal element $\rho^S_{\mu\mu}$.

Orbital	$S_z = 5$	$S_z = 0$
4s	0.080	−0.037
4p_x	0.058	−0.069
4p_y	0.032	−0.038
4p_z	0.143	−0.138
3d_{zz}	0.899	−0.877
3d_{xx-yy}	0.953	−0.954
3d_{xy}	0.852	−0.863
3d_{xz}	0.675	−0.581
3d_{yz}	0.928	−0.934

Local spin expectation values for the two components (Tables IV and V) are similar to those obtained from *ab initio* UHF calculations [3] on the hypothetical complex $[Mn_2O_2(H_2S)_2(H_2O)_2]$, which also contains (formally) high-spin d^5 ions. The expectation values obtained for the irons in $[Fe_2S_2(SH)_4]^{-2}$ are closer to the value of 8.75 expected for an isolated high-spin d^5 ion. This should not be taken as a comparison of the methods, because preliminary ZILSH calculations on larger Mn^{+2} complexes (O'Brien and Davidson, unpublished results) consistently give $\langle \hat{S}^2_{Mn} \rangle$ values of around 9.40, much closer to the values given for $[Mn_2O_2(H_2S)_2(H_2O)_2]$ in Tables IV and V. In both complexes, expectation values of the $\hat{S}^2$ operator are close to those expected for orbitally restricted Slater determinants. The spin couplings $\langle \hat{S}_{Fe(1)} \cdot \hat{S}_{Fe(2)} \rangle$ and $\langle \hat{S}_{Mn(1)} \cdot \hat{S}_{Mn(2)} \rangle$ are also similar, although the metal–metal bond orders computed for the iron complex are significantly smaller (0.11 vs. 0.39). Other bond orders show similar differences, but again direct comparison is dangerous when the atoms are different. These results indicate that the two methods are providing qualitatively similar descriptions of the electronic structure of the complexes.

When comparing local spin results computed for the two components of $[Fe_2S_2(SH)_4]^{-2}$ it is apparent that the values found for $\langle \hat{S}^2_{Fe} \rangle$ are not the same in each case. This belies the assumption that is often made that the local spins do not change with S_z of the wave function. The spin coupling $\langle \hat{S}_{Fe(1)} \cdot \hat{S}_{Fe(2)} \rangle$ is similar in magnitude for the two components. Couplings between the metal and ligand are different in some cases, for example, $\langle \hat{S}_{Fe} \cdot \hat{S}_{\mu^2-S} \rangle$ is 0.09 for the $S_z = 5$

TABLE IV

Local spin expectation values and bond orders computed for the $S_z = 5$ component of $[Fe_2S_2(SH)_4]^{-2}$.

$\langle \hat{S}^2 \rangle = 30.01$ (30.03)	Fe_1	Fe_2	$S(H)$	$H(S)$	μ_2-S	$S'(H)$	$H(S')$
Fe_1	8.70 (9.89)						
	—						
Fe_2	5.22 (5.74)	8.70 (9.79)					
	0.11 (0.39)	—					
$S(H)$	−0.24 (−0.30)	0.03 (0.00)	0.68 (1.13)				
	0.80 (0.88)	0.01	—				
$H(S)$	0.00 (−0.01)	0.00 (0.00)	−0.37 (−0.38)	0.37 (0.40)			
	0.00	0.00	0.99	—			
μ_2-S	0.09 (−0.31)	0.09 (−0.25)	0.00 (−0.01)	0.00 (0.00)	0.87 (0.96)		
	1.06 (1.28)	1.06 (1.12)	0.01	0.00	—		
$S'(H)$	0.03 (0.03)	−0.24 (−0.13)	0.00 (0.00)	0.00 (0.00)	0.00 (0.00)	0.68 (0.84)	
	0.01	0.80 (0.46)	0.00	0.00	0.01	—	
$H(S')$	0.00 (−0.01)	0.00 (−0.02)	0.00 (0.00)	0.00 (0.00)	0.00 (0.00)	−0.37 (−0.33)	0.37 (0.34)
	0.00	0.00	0.00	0.00	0.00	0.99	—

Results in parentheses are from *ab initio* UHF calculations on the similar complex $[Mn_2(\mu_2\text{-}O)_2(H_2S)_2(H_2O)_2]$ (Refs. [3] and [5]).

component and −0.33 for the $S_z = 0$ component. The bond order computed for this interaction, however, is virtually unchanged, 1.06 vs. 1.08. The change in $\langle \hat{S}_{Fe} \cdot \hat{S}_{\mu^2-S} \rangle$ is largely due to changes in the term $m_{Fe}m_S$ that occurs in Eq. (35), as can be seen from Table II. This is true for all other metal–ligand interactions as well.

The Heisenberg coupling constant $J_{Fe(1),Fe(2)}$ for this complex obtained using the energy difference of 2940 cm^{-1} and the $\langle \hat{S}_{Fe(1)} \cdot \hat{S}_{Fe(2)} \rangle$ values of Tables IV and V is −144 cm^{-1}. Cory et al. reported a value of −98 cm^{-1} for this coupling using the same wave functions, computed under the assumption of formal values of the local spins and total spin [4]. They found a value of −161 cm^{-1} using the energies of pure spin components projected out of the $S_z = 0$ UHF wave function. Clearly there is much greater similarity between the value obtained using the local spin operators (−144 cm^{-1}) and the energies of the pure spin states (−161 cm^{-1}). This is a demonstration of the conclusion of Section 3: A good approximation of

TABLE V

Local spin expectation values and bond orders computed for the $S_z = 0$ component of $[Fe_2S_2(SH)_4]^{-2}$.

$\langle \hat{S}^2 \rangle = 4.78$ (5.03)	Fe_1	Fe_2	$S(H)$	$H(S)$	μ_2-S	$S'(H)$	$H(S')$
Fe_1	8.33 (9.84)						
	—						
Fe_2	−4.95 (−5.99)	8.33 (9.82)					
	0.12	—					
$S(H)$	−0.25 (−0.30)	−0.03 (−0.04)	0.68 (1.13)				
	0.79	0.01	—				
$H(S)$	0.00 (−0.01)	0.00 (−0.01)	−0.37 (−0.38)	0.37 (0.40)			
	0.00	0.00	0.99	—			
μ_2-S	−0.33 (−0.38)	−0.33 (−0.47)	0.00 (−0.01)	0.00 (0.00)	0.84 (0.96)		
	1.08	1.08	0.01	0.00	—		
$S'(H)$	−0.03 (−0.02)	−0.25 (−0.15)	0.00 (0.00)	0.00 (0.00)	0.00 (0.00)	0.68 (0.84)	
	0.01	0.79	0.00	0.00	0.01	—	
$H(S')$	0.00 (0.00)	0.00 (−0.01)	0.00 (0.00)	0.00 (0.00)	0.00 (0.00)	−0.37 (−0.33)	0.37 (0.34)
	0.00	0.00	0.00	0.00	0.00	0.99	—

Results in parentheses are from *ab initio* UHF calculations on the similar complex $[Mn_2(\mu_2\text{-}O2(H_2S)_2(H_2O)_2]$ (Refs. [3] and [5]).

TABLE VI

Local spin expectation values, bond orders, and $\langle \hat{S}^2 \rangle$ computed for the $S_z = 5$ and $S_z = 0$ components of the complexes $[(HB(pz)_3Fe)_2O(OAc)_2]$ and $[(HB(pz)_3Fe)_2(OH)(OAc)_2]^+$.

	$[(HB(pz)_3Fe)_2O(OAc)_2]$		$[(HB(pz)_3Fe)_2(OH)(OAc)_2]^+$	
	$S_z = 0$	$S_z = 5$	$S_z = 0$	$S_z = 5$
Fe_1	8.13	8.30	8.16	8.18
	—	—	—	—
Fe_2	8.12	8.29	8.18	8.20
	—	—	—	—
μ_2-O(H)	0.90	0.91	0.95	0.96
	—	—	—	—
Fe_1, Fe_2	−4.67	4.81	−4.71	4.73
	0.07	0.06	0.02	0.01
Fe_1, μ_2-O(H)	−0.35	0.06	−0.25	−0.13
	1.15	1.10	0.75	0.75
Fe_2, μ_2-O(H)	−0.35	0.06	−0.27	−0.14
	1.14	1.09	0.76	0.76
$\langle \hat{S}^2 \rangle$	5.12	30.24	5.09	30.10

the coupling constant describing the spin states of the system can be obtained from spin-contaminated single determinant wave functions using the local spin formalism.

7.2. $[(HB(pz)_3Fe)_2O(OAc)_2]$ AND $[(HB(pz)_3Fe)_2(OH)(OAc)_2]^+$

Local spin expectation values computed for $S_z = 0$ and $S_z = 5$ UHF components of these complexes (Table VI) are similar to those obtained for $[Fe_2S_2(SH)_4]^{-2}$. In each case $\langle \hat{S}^2_{Fe} \rangle$ is slightly smaller. As seen in subsequent tables, however, these lower values are consistently obtained for complexes with oxide rather than sulfide ligands. The metal–metal spin couplings of Table VI are similar to those of Tables IV and V, as are the expectation values of $\hat{S}^2$. The latter are close to those expected for ORSDs, 5 and 30 for the antiferromagnetic and ferromagnetic cases, respectively.

It is interesting to compare coupling constants obtained for these complexes using some of the various approximations discussed above. The most approximate approach is to simply assume that the UHF wave functions are spin eigenfunctions, as was done in Ref. [4]. Another approach is that of Noodleman [24–26], in which values of $\langle \hat{S}^2 \rangle$ are taken for the UHF wave functions but the local spins are assumed to be invariant for these wave functions. As found for the previous complex, the results of Table VI indicate that this is not strictly true. A third approach is that outlined here, taking both energies and expectation values for $\hat{S}_A \cdot \hat{S}_B$ from the UHF components and solving simultaneously for the coupling constant(s). This approach gives results that are most consistent with coupling constants obtained from experiment (Table VII). The most approximate of the three approaches is to assume spin eigenfunctions. The Noodleman approach is intermediate between the other two, although perhaps more similar to the first approach. This again supports the conclusion of Section 3: The best approximation of the coupling constant that can be obtained from spin-contaminated single determinant wave functions is found using the local spin formalism.

7.3. $[Fe_3O(TIEO)_2(O_2CPh)_2Cl_3]$

Local spin expectation values for the four components of this complex (Table VIII) are similar to those discussed above. The metal–metal bond orders are close to zero, while those for interaction of the metals with the central μ^3-oxide ligand are considerably larger. The symmetry-unique metal $[Fe_{(3)}]$ has a smaller bond order with the central oxide, which correlates directly with the longer Fe—O distance, 2.07 Å compared to 1.86 Å for the other irons. The metal–oxide bond orders are virtually identical for all four components. Values of $\langle \hat{S}^2 \rangle$ are similar to those expected for

TABLE VII

Exchange constants J_{AB} computed for the complexes $[(HB(pz)_3Fe)_2O(OAc)_2]$ and $[(HB(pz)_3Fe)_2(OH)(OAc)_2]^+$ with various models (see text for details).

Quantity	$[(HB(pz)_3Fe)_2O(OAc)_2]$	$[(HB(pz)_3Fe)_2(OH)(OAc)_2]^+$
ΔE (cm^{-1})[a]	2205	290
J (cm^{-1}) (this work)	−116	−15
J (Noodleman model)[b]	−88	−12
J (assuming spin eigenfunctions)[c]	−74	−10
J (experiment)[d]	−121	−17

[a] Defined as $E(S_z = 5) - E(S_z = 0)$.
[b] Refs. [24–26].
[c] Assuming $E = E_0 - J \cdot [\langle \hat{S}^2 \rangle - \langle \hat{S}_A^2 \rangle - \langle \hat{S}_B^2 \rangle]$, $S = 5$ or $S = 0$, $S_A = S_B = 5/2$. See, e.g., Ref. [4].
[d] Ref. [81].

ORSDs, 63.75 for the high-spin component and 13.75 for the others.

Coupling constants computed using the energies and expectation values of $\hat{S}_A \cdot \hat{S}_B$ from Table VIII are $J_{12} = -52$ cm^{-1}, $J_{13} = -16$ cm^{-1}, and $J_{23} = -15$ cm^{-1}. These values compare well with those obtained by fitting to variable-temperature magnetic susceptibility data, $J_{12} = -55$ cm^{-1}, $J_{13} \approx J_{23} = -8$ cm^{-1}. The slight discrepancy between J_{13} and J_{23} found here arises because the triangle formed by the metals is only approximately isosceles. Even though the correct trend in the magnitudes of J_{12} and J_{13} is obtained, J_{13} is enough too large relative to J_{12} that the HSM predicts the wrong ground state with the calculated coupling constants. According to the experimental data, the ground state of the complex has a total spin of $5/2$, in which the coupling J_{12}

TABLE VIII

Local spin expectation values, bond orders, energies, and $\langle \hat{S}^2 \rangle$ computed for various components of the complex $[Fe_3O(TIEO)_2(O_2CPh)_2Cl_3]$.

	$S_z = 15/2\,(\uparrow\uparrow\uparrow)$	$S_z = 5/2\,(\downarrow\uparrow\uparrow)$	$S_z = 5/2\,(\uparrow\downarrow\uparrow)$	$S_z = 5/2\,(\uparrow\uparrow\downarrow)$
Fe_1	8.27	8.16	8.16	8.26
	—	—	—	—
Fe_2	8.26	8.16	8.15	8.25
	—	—	—	—
Fe_3	8.30	8.27	8.27	8.25
	—	—	—	—
μ_3-O	0.97	0.96	0.96	0.96
	—	—	—	—
Fe_1-Fe_2	4.79	−4.70	−4.69	4.78
	0.03	0.03	0.03	0.03
Fe_1-Fe_3	4.79	−4.73	4.73	−4.77
	0.03	0.02	0.02	0.02
Fe_2-Fe_3	4.79	4.73	−4.73	−4.77
	0.02	0.02	0.02	0.02
Fe_1-(μ_3-O)	−0.07	−0.37	−0.22	−0.23
	0.88	0.89	0.89	0.88
Fe_2-(μ_3-O)	−0.07	−0.22	−0.38	−0.23
	0.88	0.88	0.89	0.88
Fe_3-(μ_3-O)	0.00	−0.15	−0.15	−0.30
	0.68	0.68	0.68	0.68
Energy (cm^{-1})	1282.6	0.0	3.7	691.1
$\langle \hat{S}^2 \rangle$	65.37	15.32	15.31	15.33

S_z for each metal is represented by an up arrow ($S_{zA} = 5/2$) or down arrow ($S_{zA} = -5/2$). $Fe_{(3)}$ is symmetry unique (see Fig. 1).

dominates the smaller couplings across the legs of the triangle. In this case the spins of $Fe_{(1)}$ and $Fe_{(2)}$ couple to give a resultant of zero. The wave function for this state in the notation of Eq. (6) is

$$\left|S=\frac{5}{2},\,S_z=\frac{5}{2}\right\rangle=\frac{1}{\sqrt{6}}\left[\begin{array}{l}\left|\frac{5}{2}\,\frac{5}{2}\right\rangle\left|\frac{5}{2}\,-\frac{5}{2}\right\rangle\left|\frac{5}{2}\,\frac{5}{2}\right\rangle+\left|\frac{5}{2}\,\frac{3}{2}\right\rangle\left|\frac{5}{2}\,-\frac{3}{2}\right\rangle\left|\frac{5}{2}\,\frac{5}{2}\right\rangle+\left|\frac{5}{2}\,\frac{1}{2}\right\rangle\left|\frac{5}{2}\,-\frac{1}{2}\right\rangle\left|\frac{5}{2}\,\frac{5}{2}\right\rangle\\ -\left|\frac{5}{2}\,-\frac{1}{2}\right\rangle\left|\frac{5}{2}\,\frac{1}{2}\right\rangle\left|\frac{5}{2}\,\frac{5}{2}\right\rangle-\left|\frac{5}{2}\,-\frac{3}{2}\right\rangle\left|\frac{5}{2}\,\frac{3}{2}\right\rangle\left|\frac{5}{2}\,\frac{5}{2}\right\rangle-\left|\frac{5}{2}\,-\frac{5}{2}\right\rangle\left|\frac{5}{2}\,\frac{5}{2}\right\rangle\left|\frac{5}{2}\,\frac{5}{2}\right\rangle\end{array}\right],\qquad(54)$$

which gives a total S_z of 0 for $Fe_{(1)}$ and $Fe_{(2)}$ and $S_z = 5/2$ for $Fe_{(3)}$. The first excited state has a total spin of $3/2$, resulting from an incomplete pairing of the spins of $Fe_{(1)}$ and $Fe_{(2)}$. The couplings in these states of a trinuclear complex are well understood based on the concept of spin frustration (see Libby et al. [97] for a lucid discussion). When the ratio of J_{13} to J_{12} becomes large enough, the state with $S = 3/2$ becomes the ground state, as J_{12} is no longer large enough to completely frustrate J_{13} and J_{23}. This is the situation with the computed values of these coupling constants: J_{13} is just large enough relative to J_{12} to make the $S = 3/2$ state the ground state by about four wave numbers. The $S = 5/2$ state becomes the ground state when the ratio J_{13}/J_{12} is just under one third, so if J_{13} and J_{23} were even two wave numbers lower in energy the correct ground state would be obtained. As discussed below, the correct ground state is obtained for the other nine complexes considered.

Although J_{13} estimated by the calculations is twice as large as J_{13} as fit by Gorun et al. [83], the difference is small in absolute terms for a method like INDO/S. This method is known to have an accuracy of 1000–2000 cm^{-1} for optical transition energies of molecules ranging from aromatic heterocycles to transition metal complexes [16]. Although the accuracy of INDO/S for transition metal complexes has never been systematically examined, the general feeling is that the method is in particular accurate for $d \rightarrow d$ transitions [9, 16, 52]. Thus, it may not be unreasonable to assume an accuracy of 500 cm^{-1} for these cases. Even so, errors of this size in state energies could entail significant errors in the values obtained for exchange constants. With this in mind, we consider the discrepancy of 8 cm^{-1} in the values of $J_{13} \approx J_{23}$ to be small. Although the energies of the $S = 3/2$ and $S = 5/2$ states discussed above are inverted, the calculated values of the coupling constants give a qualitatively correct description of the magnetic interactions in this complex.

7.4. $[Fe_4O_2(OAc)_7(bpy)_2]^+$ AND $[Fe_4O_2Cl_2(OAc)_6(bpy)_2]$

Local spin expectation values and bond orders computed for the UHF, $S_z = 0$ components of these complexes (Table IX) are again similar to those obtained for the previously considered cases. The bond order between the wingtip irons and μ_3-oxide ions is larger than that between the body irons and μ_3-oxides. This again correlates with the Fe—O distance: In $[Fe_4O_2(OAc)_7(bpy)_2]^+$, for example, the distance between $Fe_{(1)}$ and $O_{(5)}$ is close to 1.82 Å, while the $Fe_{(2)}$—$O_{(5)}$ distance is roughly 1.95 Å. It is interesting to compare coupling constants computed for these two complexes because $[Fe_4O_2(OAc)_7(bpy)_2]^+$ has a more symmetrical core than $[Fe_4O_2Cl_2(OAc)_6(bpy)_2]$ does, yet it was assumed for both complexes that all four J_{wb} interactions were equal when fitting to variable-temperature magnetic susceptibility data [82, 107] (Figs. 2 and 3). $[Fe_4O_2(OAc)_7(bpy)_2]^+$ has inversion symmetry, and this is reflected in the values obtained for the coupling constants (Table IX): There are two distinct values for J_{wb} but they are similar. In this case the approximation of equating all J_{wb} is valid. In $[Fe_4O_2Cl_2(OAc)_6(bpy)_2]$, on the other hand, the core is asymmetrical in terms of Fe—Fe distances and ligands. The four J_{wb} couplings computed for this complex are different, ranging from -32 to -60 cm^{-1}. In such asymmetrical cases, care should be taken when making assumptions about the coupling constants, although it should be noted that the two sets of coupling constants listed for this complex give similar ground-state properties when substituted into the HSH (see Table XIII and the discussion below).

For both complexes it was found that the value of J_{bb} was "indeterminate" from the fit to variable-temperature magnetic susceptibility data [82, 107]. It was found for $[Fe_4O_2(OAc)_7(bpy)_2]^+$ that values of J_{bb} ranging from -15 to $+105$ cm^{-1} gave the same relative error in the fit. This occurs because J_{wb} is so much larger than J_{bb} that the value of J_{bb} does not affect states with energies less than 300 K.

TABLE IX

Local spin expectation values, bond orders, and Heisenberg coupling constants computed for the $S_z = 0$ UHF components of the complexes $[Fe_4O_2(OAc)_7(bpy)_2]^+$ and $[Fe_4O_2Cl_2(OAc)_6(bpy)_2]$.

	Complex					
	$[Fe_4O_2(OAc)_7(bpy)_2]^+$			$[Fe_4O_2Cl_2(OAc)_6(bpy)_2]$		
Parameter	$\langle \hat{S}_A \cdot \hat{S}_B \rangle$	B_{AB}	J (cm^{-1})	$\langle \hat{S}_A \cdot \hat{S}_B \rangle$	B_{AB}	J (cm^{-1})
Fe_1	8.20	—	—	8.19	—	—
Fe_2	8.23	—	—	8.23	—	—
Fe_3	8.22	—	—	8.28	—	—
Fe_4	8.20	—	—	8.12	—	—
O_5	0.97	—	—	0.97	—	—
O_6	0.97	—	—	0.98	—	—
Fe_1-O_5	−0.40	0.99	—	−0.37	1.02	—
Fe_2-O_5	−0.15	0.73	—	−0.18	0.72	—
Fe_3-O_5	−0.14	0.70	—	−0.19	0.71	—
Fe_4-O_6	−0.40	0.99	—	−0.39	1.00	—
Fe_2-O_6	−0.14	0.70	—	−0.18	0.73	—
Fe_3-O_6	−0.15	0.73	—	−0.19	0.73	—
Fe_1-Fe_2	−4.71	0.04	−58 (−45)	−4.71	0.04	−60 (−41)
Fe_1-Fe_3	−4.71	0.03	−61 (−45)	−4.74	0.03	−51 (−41)
Fe_2-Fe_4	−4.71	0.03	−61 (−45)	−4.69	0.03	−57 (−41)
Fe_3-Fe_4	−4.71	0.04	−58 (−45)	−4.72	0.03	−32 (−41)
Fe_2-Fe_3	4.70	0.02	−6 (−9)	4.73	0.02	−9 (−11)
Fe_1-Fe_4	4.71	0.00	−1 (0)	4.69	0.00	−1 (0)

Values in parentheses from fits to reproduce variable-temperature magnetic susceptibility measurements (Refs. [82] and [107], respectively). See Figures 2 and 3 for numbering schemes.

McCusker et al. thus concluded that J_{bb} is greater than -15 cm^{-1} and probably antiferromagnetic [82]. A similar situation is obtained for $[Fe_4O_2Cl_2(OAc)_6(bpy)_2]$ [107]. In both cases the ZILSH calculations support this hypothesis, with estimates of -6 and -9 cm^{-1}, respectively. It is also interesting to note that the coupling J_{ww} that was neglected in both fits [82, 107] is predicted to have a small but nonzero value of -1 cm^{-1} in each case.

Substitution of the coupling constants of Table IX into the HSH predicts similar ground states with $S = 0$ for each complex (Table XIII). In both of these singlet states, the ground-state wave function is a linear combination of many pairs of components with reversed spins [as in Eq. (53)], leading to $S_z(Fe_x)$ of zero for all metals. The two largest coefficients (which are equal with squares on the order of 0.10) lead the components $|5/2\,5/2\rangle|5/2\ -\ 5/2\rangle|5/2\ -\ 5/2\rangle|5/2\,5/2\rangle$ and $|5/2\ -\ 5/2\rangle|5/2\,5/2\rangle|5/2\,5/2\rangle|5/2\ -\ 5/2\rangle$. Wave functions obtained with the calculated and experimental coupling constants are similar. In both cases, the spins of the body irons are aligned parallel, as are the wingtip ion spins, despite the inherently antiferromagnetic nature of these couplings. This is an example of spin frustration, in which the much larger J_{wb} couplings dominate.

7.5. $[Fe_4(OCH_3)_6(dpm)_6]$

Local spin expectation values and bond orders (Table X) for this SMM are again similar to the results of the previous tables. The Fe—O(Me) bond orders of ~0.70 are typical for Fe—O bonds with distances on the order of 1.95 Å. The metal–metal spin couplings lead to estimates of coupling constants that agree well with those predicted by fitting to variable-temperature magnetic susceptibility data (Table X). Next-nearest-neighbor couplings obtained from the calculations are small but antiferromagnetic, while those from the fit are slightly ferromagnetic. In both cases their magnitude is too small to influence the spin-state energies or wave functions. The ground state predicted with the HSM using both sets of Js has a total spin of five (Table XIII), with $Fe_{(1)-(3)}$ all antiferromagnetically coupled to the spin of the central $Fe_{(4)}$. The values of $S_z(Fe_x)$ are reduced below the formal magnitude of five by mixing of components with $|S_{zA}|$ less than five. The leading contribution is from the compo-

TABLE X

Local spin expectation values, bond orders, and Heisenberg coupling constants computed for the $S_z = 5$ UHF component of the complex $[Fe_4(OCH_3)_6(dpm)_6]$.

Parameter	$\langle \hat{S}_A \cdot \hat{S}_B \rangle$	B_{AB}	J (cm^{-1})
Fe_1	8.24	—	—
Fe_2	8.24	—	—
Fe_3	8.25	—	—
Fe_4	8.35	—	—
O_5	0.94	—	—
O_6	0.94	—	—
Fe_1-O_5	−0.22	0.71	—
Fe_1-O_6	−0.22	0.71	—
Fe_4-O_5	−0.23	0.69	—
Fe_4-O_6	−0.24	0.68	—
Fe_1-Fe_4	−4.75	0.01	−36.8 (−21.1)
Fe_2-Fe_4	−4.75	0.01	−36.8 (−21.1)
Fe_3-Fe_4	−4.76	0.01	−36.5 (−21.1)
Fe_1-Fe_2	4.71	0.00	−0.1 (+1.1)
Fe_1-Fe_3	4.72	0.00	−0.1 (+1.1)
Fe_2-Fe_3	4.72	0.00	−0.1 (+1.1)

Values in parentheses from fit to reproduce variable-temperature magnetic susceptibility measurements (Ref. [108]). See Figure 4 for numbering scheme.

nent $|5/2\ 5/2\rangle|5/2\ 5/2\rangle|5/2\ 5/2\rangle|5/2\ -\ 5/2\rangle$ with a coefficient of 0.83 for both sets of coupling constants.

7.6. $[Fe_6O_2(hmp)_8Cl_4]^{+2}$ AND $[Fe_6O_2(OH)_2(OAc)_{10}(C_{10}H_{13}N_4O)_2]$

These complexes have topologically similar core structures (Figs. 6 and 7). Both complexes have inversion symmetry. Local spin expectation values and bond orders (Table XI) are similar to those found for the other complexes. Christmas et al. [84] suggested that there are four nonzero symmetry-unique exchange couplings in these complexes, J_{12}, J_{13}, J_{23}, and J_{24} (see Figs. 5 and 6 for numbering schemes). Other couplings related to these by the inversion operation carry the same values. The ZILSH calculations confirm that couplings between all other metals in both complexes are close to zero. For the cation, it was further assumed that $J_{12} = J_{13}$ when fitting to reproduce variable-temperature magnetic susceptibility data, which appears to be a mild approximation: Calculated values for these couplings agree to within a wave number and agree with the fit values within 10 wave numbers. Good agreement is also obtained for J_{23}, but a large difference between the calculated and fit value of J_{24} is found, -40 cm^{-1} vs. -3 cm^{-1}, respectively.

When considering this discrepancy, it is instructive to note that antiferromagnetic couplings between oxide-bridged Fe^{+3} ions of less than 10 cm^{-1} are well known, as in the J_{bb} interactions discussed above for $[Fe_4O_2(OAc)_7(bpy)_2]^+$ and $[Fe_4O_2Cl_2(OAc)_6(bpy)_2]$. In these cases the Fe—Fe distance is typically short, on the order of 2.90 Å, while the Fe_2—Fe_4 distance in $[Fe_6O_2(hmp)_8Cl_4]^{+2}$ is longer, 3.166 Å (Fig. 5). The bridging between Fe_2 and Fe_4 by the alkoxide functional groups of the bidentate hmp^- ligands bears a closer resemblance to the situation in $[Fe_4(OMe)_6(dpm)_6]$, where Fe_1 and Fe_4 are bridged by two OMe^- ligands. The Fe—Fe distances are 3.133 Å in $[Fe_4(OMe)_6(dpm)_6]$ and 3.166 Å in $[Fe_6O_2(hmp)_8Cl_4]^{+2}$ and Fe-O-Fe angles are 104 and 105°, respectively. The Fe—Fe exchange constant in $[Fe_4(OMe)_6(dpm)_6]$ is considerably larger, -21 cm^{-1} (Table X). Also, the values of all other coupling constants considered in this article were estimated with an accuracy of better than 20 cm^{-1} (considerably better in the majority of cases) by the calculations, while in this case the discrepancy is 37 cm^{-1}. A value of -3 cm^{-1} seems small given these considerations. However, it is difficult to judge the inherent accuracy of the ZILSH method based on the few test cases examined here as there is virtually no experience with the INDO/S model applied to complexes with multiple metal centers, and it is true that the fit values reproduce the variable-temperature magnetic susceptibility data accurately. It is possible that the method is simply providing a poor estimate of this coupling. Another possibility that should be considered is that there could be other sets of coupling constants that also fit the magnetization data. The curves produced by these experiments have straightforward shapes that might easily be reproduced by several sets of constants. We made preliminary observations of this behavior for fits for tetranuclear manganese complexes (O'Brien and Davidson, unpublished results) using a genetic algorithm program. This question of the validity of different fits to magnetization data could be the subject of future work.

Despite the large discrepancy in the values found for J_{24}, both the calculated and fit coupling constants yield the same ground state when used in the HSH (Table XIII). The ground state is a singlet in both cases. As with the other singlet states discussed above [see Eq. (53)], the wave function for this state is a linear combination of many components, each with a small coefficient, with pairs of

TABLE XI

Local spin expectation values, bond orders, and Heisenberg coupling constants computed for the $S_z = 0$ UHF component of $[Fe_6O_2(hmp)_8Cl_4]^{+2}$ and the $S_z = 5$ UHF component of $[Fe_6O_2(OH)_2(OAc)_{10}(C_{10}H_{13}N_4O)_2]$.

Complex	$[Fe_6O_2(hmp)_8Cl_4]^{+2}$			$[Fe_6O_2(OH)_2(OAc)_{10}(C_{10}H_{13}N_4O))_2]$		
Parameter	$\langle \hat{S}_A \cdot \hat{S}_B \rangle$	B_{AB}	J (cm^{-1})	$\langle \hat{S}_A \cdot \hat{S}_B \rangle$	B_{AB}	J (cm^{-1})
Fe_1	8.21	—	—	8.33	—	—
Fe_2	8.09	—	—	8.36	—	—
Fe_3	8.14	—	—	8.33	—	—
Fe_4	8.11	—	—	8.33	—	—
Fe_5	8.12	—	—	8.36		
Fe_6	8.21	—	—	8.33		
O_7	0.97	—	—	0.96	—	—
O_8	0.97	—	—	0.96	—	—
O_9	0.96	—	—	0.94		
Fe_1-O_7	−0.17	0.79	—	−0.18	0.84	—
Fe_2-O_7	−0.37	0.84	—	−0.14	0.73	—
Fe_3-O_7	−0.19	0.83	—	−0.37	0.83	—
Fe_2-O_9	−0.27	0.74	—	−0.23	0.73	—
Fe_4-O_9	−0.22	0.72	—	−0.23	0.69	—
Fe_1-Fe_2	−4.69	0.02	−24 (−18)	4.80	0.02	−19 (−6)
Fe_1-Fe_3	4.71	0.02	−26 (−18)	−4.79	0.03	−41 (−38)
Fe_2-Fe_3	−4.63	0.02	−53 (−52)	−4.80	0.02	−52 (−38)
Fe_2-Fe_4	−4.61	0.01	−40 (−3)	−4.80	0.02	−26 (−8)

Values in parentheses from fits to reproduce variable-temperature magnetic susceptibility measurements (Ref. [84]). Interactions with zero magnitude and certain symmetry-equivalent interactions omitted. See Figures 5 and 6 for numbering schemes.

components with local z-components of spin reversed that have coefficients that are equal and opposite in sign. The result is a local z-component of spin of zero for each metal, as shown in Table XIII. This reflects the fundamental structure of singlet spin eigenfunctions. In the ground-state wave function of $[Fe_6O_2(hmp)_8Cl_4]^{+2}$, the components $|5/2\,5/2\,-5/2\,-5/2\,5/2\,-5/2\rangle$ and $|-5/2\,-5/2\,5/2\,5/2\,-5/2\,5/2\rangle$ make a slightly larger contribution than any others. Here, the more compact notation $|S_{z1}S_{z2}S_{z3}S_{z4}S_{z5}S_{z6}\rangle$ has been adopted. These combinations of local z-components of spin can be understood by considering the magnitudes of the exchange constants, with J_{23} much larger than the other nonzero constants.

Coupling constants obtained for $[Fe_6O_2(OH)_2(OAc)_{10}(C_{10}H_{13}N_4O)_2]$ (Table XI) do not display a large deviation from fit values, as was found for $[Fe_6O_2(hmp)_8Cl_4]^{+2}$. The value of J_{24} estimated by the calculations still shows a somewhat large deviation from the fit value, 18 cm^{-1}, although not nearly as large as the deviation found for the other complex. In this case, Christmas et al. [84] assumed that $J_{13} = J_{23}$ even though the Fe_1-Fe_2-Fe_3 triangle is obviously scalene (see Fig. 6). A value of -38 cm^{-1} was obtained from the fit to magnetic susceptibility data. The calculations give values of -41 and -52 cm^{-1}, indicating that J_{13} and J_{23} are not in fact all that similar. The calculated values of the coupling constants show the same trend in magnitude shown by the experimental values. Both calculated and fit exchange constants indicate a ground state with a total spin of five when substituted into the HSH. In both cases the leading contribution to the wave function is from the component $|5/2\,5/2\,-5/2\,-5/2\,5/2\,5/2\rangle$, with a coefficient of 0.66 and 0.63 for calculated and fit coupling constants, respectively. Again, this distribution of local z-components of spin can be rationalized based on the relative magnitudes of the coupling constants.

7.7. $[Fe_6O_3(OAc)_9(OEt)_2(bpy)_2]^+$

Up to now, only complexes for which values of coupling constants have been obtained from fits to reproduce variable-temperature magnetic susceptibility data have been considered. This was done to provide a basis for comparison with calculated estimates of the constants. Although a variable-temperature magnetic susceptibility study was carried

TABLE XII

Local spin expectation values, bond orders, and Heisenberg coupling constants computed for the $S_z = 0$ UHF component of the complex $[Fe_6O_3(OAc)_9(OEt)_2(bpy)_2]^+$.

Parameter	$\langle \hat{S}_A \cdot \hat{S}_B \rangle$	B_{AB}	J (cm^{-1})
Fe_1	8.26	—	—
Fe_2	8.27	—	—
Fe_3	8.32	—	—
Fe_4	8.27	—	—
Fe_5	8.30		
Fe_6	8.24		
O_7	0.97	—	—
O_8	1.04	—	—
Fe_1-O_7	−0.40	0.97	—
Fe_2-O_7	−0.15	0.73	—
Fe_3-O_7	−0.15	0.74	—
Fe_2-O_8	−0.21	0.64	—
Fe_3-O_8	−0.20	0.63	—
Fe_4-O_8	−0.20	0.64	—
Fe_5-O_8	−0.20	0.63	—
Fe_1-Fe_2	−4.75	0.03	−48
Fe_1-Fe_3	−4.77	0.03	−53
Fe_2-Fe_3	4.75	0.02	−4
Fe_4-Fe_5	4.74	0.02	−3
Fe_4-Fe_6	−4.74	0.03	−56
Fe_5-Fe_6	−4.75	0.03	−49
Fe_2-Fe_4	−4.74	0.02	−10
Fe_2-Fe_5	−4.75	0.02	−55
Fe_3-Fe_4	−4.76	0.01	−25
Fe_3-Fe_5	−4.77	0.01	−10

Interactions that are approximately symmetry equivalent are omitted. See Figure 7 for numbering scheme.

out for this complex [114], no attempt was made to fit coupling constants due to the number of interactions that would have to be considered (10 in all; see Fig. 7 and Table XII) and the lack of molecular symmetry. This complex was chosen as the final test case to demonstrate the potential of the ZILSH method to aid in understanding the magnetic interactions in complexes with low symmetry and large numbers of couplings. The method makes no assumptions regarding the magnitudes or signs of any couplings, nor are any couplings assumed to be zero. A case such as this is no more difficult to treat by the method developed in this article than the other, simpler cases considered above were. Because the ZILSH method can also be applied to larger complexes (we already performed calculations on complexes with up to 12 metals, to be presented at a later time), it has great potential to contribute to the study of magnetic interactions in polynuclear transition metal complexes.

Although exchange constants were not fit to reproduce the variable-temperature magnetic susceptibility data for this complex, Seddon et al. [114] predicted based on the shape of the curve that the total spin of the complex is zero. By considering the structure and nature of the bridging ligands, they were also able to make general predictions regarding the magnetic couplings. The two triangles defined by (Fe_1-Fe_2-Fe_3) and (Fe_4-Fe_5-Fe_6) resemble triangles found in tetranuclear butterfly complexes. For example, Fe_2 and Fe_3 are bridged by two oxide ions and have a short metal–metal distance, 2.96 Å (Fig. 7). The Fe_1–Fe_2 and Fe_1–Fe_3 interactions resemble wingtip-body couplings in the butterfly complexes, bridged by a μ_3-oxide ligand and with metal–metal distances of ~3.3 Å. On this basis it was predicted that J_{23} would be small, on the order of $-10\ cm^{-1}$ or less, and J_{12} and J_{13} larger, on the order of $50\ cm^{-1}$ judging by the two butterfly complexes considered above. This general picture is supported by the calculated coupling constants for the two triangles (Table XII): J_{23} and J_{45} are on the order of $-5\ cm^{-1}$, while the four "J_{wb}" couplings are on the order of $-50\ cm^{-1}$. The final four exchange constants listed in Table XII describe interactions across the central μ_4-oxide bridge. These values correlate strongly with the Fe-(μ_4-O)-Fe bond angles, which are highly variable, ranging from 94.0 to 156.9°.

When substituted into the HSH, the coupling constants of Table XII yield a ground state with $S = 0$ (Table XIII), as suggested by Seddon et al. [114] on the basis of variable-temperature magnetic susceptibility data. They predicted that the spins of this complex would align as shown in Figure 7, with the "J_{bb}" interactions (J_{23} and J_{45}) frustrated due to the larger interactions in the complex. Because the ground state is a singlet, in actuality the local z-components of spin of the metals are zero because the wave function is a linear combination of a number of equally weighted pairs of components with reversed z-components of spin. The largest coefficients (±0.23) lead the components $|5/2\ -\ 5/2\ -\ 5/2\,5/2\,5/2\ -\ 5/2\rangle$ and $|-5/2\,5/2\,5/2\ -\ 5/2\ -\ 5/2\,5/2\rangle$, which display the orientation of spins predicted by Seddon et al.

8. Conclusions and Future Directions

The local spin formalism [3, 5] has been extended to semiempirical single determinant wave func-

TABLE XIII

Properties of ground states of tetranuclear and hexanuclear complexes computed with the HSH for various complexes.

Complex	Spin of ground state	Leading contribution[a]	S_z (Fe_1)	S_z (Fe_2)	S_z (Fe_3)	S_z (Fe_4)	S_z (Fe_5)	S_z (Fe_6)
$[Fe_4O_2(OAc)_7(bpy)_2]^+$	0	↑ ↓ ↓ ↑	0	0	0	0	—	—
	(0)	(↑ ↓ ↓ ↑)	(0)	(0)	(0)	(0)		
$[Fe_4O_2Cl_2(OAc)_6(bpy)_2]$	0	↑ ↓ ↓ ↑	0	0	0	0	—	—
	(0)	(↑ ↓ ↓ ↑)	(0)	(0)	(0)	(0)		
$[Fe_4(OCH_3)_6(dpm)_6]$	5	↑ ↑ ↑ ↓	4.72	4.72	4.72	−4.17	—	—
	(5)	(↑ ↑ ↑ ↓)	(4.72)	(4.72)	(4.72)	(−4.17)		
$[Fe_6O_2(C_6H_6NO)_8Cl_4]^{+2}$	0	↑ ↑ ↓ ↓ ↑ ↓	0	0	0	0	0	0
	(0)	(↑ ↑ ↓ ↓ ↑ ↓)	(0)	(0)	(0)	(0)	(0)	(0)
$[Fe_6O_2(OH)_2(OAc)_{10}(C_{10}H_{13}N_4O)_2]$	5	↑ ↑ ↓ ↓ ↑ ↑	4.67	4.31	−3.97	−3.97	4.31	4.67
	(5)	(↑ ↑ ↓ ↓ ↑ ↑)	(4.45)	(4.46)	(−3.91)	(−3.91)	(4.46)	(4.45)
$[Fe_6O_3(OAc)_9(Oet)_2(bpy)_2]^+$	0	↑ ↓ ↓ ↑ ↑ ↓	0	0	0	0	0	0

Calculated exchange constants given in Tables IX–XII were used in all cases. Values in parentheses obtained using exchange constants from fits to variable-temperature magnetization data given in Tables IX–XI. See Figures 2–7 for numbering schemes.
[a] Singlet states are linear combinations of pairs of determinants with reversed z-components of spin with equal weighting, resulting in S_z (Fe_x) = 0.00 for all metals. Only one determinant is given as leading contribution for singlets. See text for discussion.

tions. Expressions for the local spin expectation values $\langle \hat{S}_A \cdot \hat{S}_B \rangle$ that appear in the Heisenberg model of magnetism were derived assuming the ZDO approximation and implemented in the ZINDO program. This allows computation of local spins for RHF and UHF wave functions obtained from a variety of semiempirical models, including the well-known INDO/S [7, 9, 15, 16], AM1 [32], and PM3 [35, 36] methods. Expectation values obtained for polynuclear iron complexes with the INDO/S model approximately demonstrate the features of the Heisenberg spin model, with large local spin expectation values found for the irons that resemble formal values expected for isolated high-spin metals. The values were also found to be largely but not entirely invariant to reversal of spins of one or more metals.

Local spin expectation values found for the iron complexes with the INDO/S model are also similar to those obtained from *ab initio* UHF calculations on the complex $[Mn_2O_2(H_2S)_2(H_2O)_2]$, although direct comparison is difficult because the metals and oxidation states are different. There is not yet much experience with local spin in polynuclear transition metal complexes for *ab initio*, DFT, or semiempirical models. Future comparisons of these different approaches will be necessary to judge their strengths and weaknesses.

A formal connection between the Heisenberg spin model and single determinant wave functions was established. The HSM assumes a basis of states of the total spin defined by coupling of atomic spins assigned formal high-spin values. Single determinant wave functions, on the other hand, are typically not eigenfunctions of either the total spin or the local spin operators. Single determinants are "contaminated" by contributions from states with spins greater than S_z of the determinantal wave function. These spin states are in general not restricted to those specified by the HSM (i.e., those in which the atoms have their maximum local spin). It was demonstrated that if the single determinant is an eigenfunction of the local spin operators $\hat{S}_A^2$ then all spin components contributing to the single determinant are as well and have the same local spin quantum numbers. If the local spin quantum numbers of a single determinant are high spin, then all spin states contributing to that determinant are states described by the Heisenberg model. That being the case, the energy of the single determinant wave function is described by the same coupling constants $\{J_{AB}\}$ that describe the true spin states of the system.

In practice, single determinant wave functions for transition metal complexes resemble high-spin eigenfunctions of the local spin operators when the metal d orbitals are largely local in character and when all electrons in the d orbitals of each metal have the same spin (although spins on different metals can be parallel or antiparallel in alignment).

In these cases, accurate estimates of the coupling constants can be solved for simultaneously using energies and local spin expectation values computed for a set of single determinant wave functions in which spins of different metals are reversed. Substitution of the coupling constants obtained in this way into the Heisenberg Hamiltonian and diagonalization yields predictions for the energies and compositions of all spin states specified by the HSM. This allows access to spin states by means of semiempirical single determinant wave functions that can feasibly be obtained for large polynuclear complexes.

A computational method for obtaining coupling constants and spin-state energies for large polynuclear transition metal complexes using the INDO/S model has been introduced. It consists of, first, a strategy for obtaining UHF wave functions that resemble high-spin eigenfunctions of local spin for the metals of the complex; second, an automated procedure for running all necessary UHF calculations [equal in number to $1/2\,N_m(N_m - 1) + 1$, where N_m is the number of metals], extracting energies and local spin expectation values for each component, and solving simultaneously for the coupling constants; and third, diagonalization of the HSH to yield the final spin-state energies and compositions. Details can be found in Sections 4 and 5. The new method is referred to as ZILSH, derived from ZINDO, local spin, and the Heisenberg spin model.

The ZILSH method was tested on 10 complexes containing from 2 to 6 Fe^{+3} ions. Coupling constants obtained for three dinuclear complexes were compared to constants obtained using other reconciliations of quantum chemistry and the HSM, including the Noodleman approach [24–26]. Values obtained from ZILSH compared more closely with values obtained by fitting constants to reproduce variable-temperature magnetic susceptibility curves. For larger complexes, coupling constants agreed reasonably well with fit values for most exchange interactions studied and the correct spin was predicted for the ground state in 9 of 10 cases. In the other case, the ground state was about four wave numbers below the state found to be the ground state by experiment.

The coupling constants of the complex $[Fe_6O_3(OAc)_9(OEt)_2(bpy)_2]^+$ were also predicted. Although this complex was characterized by a variable-temperature magnetic susceptibility experiment [114], coupling constants were not fit to reproduce the curve due to the asymmetry of the complex and large number of nonzero exchange pathways. The predicted constants indicate a diamagnetic ground state, in agreement with experiment. Spin alignments in this ground state agree with an earlier proposal [114] made by comparing the structure of the complex to structures of smaller complexes with known coupling constants. This demonstrates the potential of the ZILSH method to elucidate magnetic interactions that are not amenable to fitting to variable-temperature magnetic susceptibility curves due to large size and/or structural intricacy of a complex. The method also can be applied to complexes that are too large to be described with more accurate *ab initio* and DFT methods. In the near future we hope to present results for polynuclear complexes relevant to nanoscale magnetism, such as $[Fe_8O_2(OH)_{12}(tacn)_6]^{+8}$.

ACKNOWLEDGMENTS

This work was supported by Grant CHE-9982415 from the National Science Foundation. The authors acknowledge Cristina Cañada-Vilalta of Indiana University for critical reading of the article prior to submission. T.A.O. acknowledges Dr. Marshall Cory of the Quantum Theory Project at the University of Florida for helpful discussions of the ZINDO code.

References

1. Aubin, S. M. J.; Wemple, M. W.; Adams, D. M.; Tsai, H.-L.; Christou, G.; Hendrickson, D. N. J Am Chem Soc 1996, 118, 7746.
2. Aubin, S. M. J.; Dilley, N. R.; Pardi, L.; Krzystek, J.; Wemple, M. W.; Brunel, L.-C.; Maple, M. B.; Christou, G.; Hendrickson, D. N. J Am Chem Soc 1998, 120, 4991.
3. Clark, A. E.; Davidson, E. R. J Chem Phys 2001, 115, 7382.
4. Cory, M. G.; Stavrev, K. K.; Zerner, M. C. Int J Quantum Chem 1997, 63, 781.
5. Davidson, E. R.; Clark, A. E. Mol Phys 2002, 100, 373.
6. Zerner, M. C.; Ridley, J. E.; Bacon, A. D.; Edwards, W. D.; Head, J. D.; McKelvey, J.; Culberson, J. C.; Knappe, P.; Cory, M. G.; Weiner, B.; Baker, J. D.; Parkinson, W. A.; Kannis, D.; Yu, J.; Rösch, N.; Kotzian, M.; Tamm, T.; Karelson, M. M. Zheng, X.; Pearl, G. M.; Broo, A.; Albert, K.; Cullen, J. M.; Cramer, C. J.; Truhlar, D. G.; Li, J.; Hawkins, G. D.; Liotard, D. A. ZINDO—A Semi-Empirical Program Package; University of Florida: Gainesville, FL, 2000.
7. Ridley, J.; Zerner, M. C. Theor Chim Acta 1973, 32, 111.
8. Bacon, A. D.; Zerner, M. C. Theor Chim Acta 1979, 53, 21.
9. Zerner, M. C.; Loew, G. H.; Kirchner, R. F.; Mueller-Westerhoff, U. T. J Am Chem Soc 1980, 102, 589.
10. Anderson, W. P.; Cundari, T.; Drago, R. S.; Zerner, M. C. Inorg Chem 1990, 29, 1.

11. Anderson, W. P.; Cundari, T. R.; Zerner, M. C. Int J Quantum Chem 1991, 39, 31.
12. Culberson, J. C.; Knappe, P.; Rösch, N.; Zerner, M. C. Theor Chim Acta 1987, 71, 21.
13. Kotzian, M.; Rösch, N.; Zerner, M. C. Theor Chim Acta 1992, 81, 201.
14. Cory, M. G.; Kostlmeier, S.; Kotzian, M.; Rösch, N.; Zerner, M. C. J Chem Phys 1994, 100, 1353.
15. Martin, C. H.; Zerner, M. C. In Inorganic Electronic Structure and Spectroscopy, Vol. 1; Solomon, E. I.; Lever, A. B. P., Eds.; John Wiley & Sons: New York, 1999, p. 555.
16. Zerner, M. C. In Reviews in Computational Chemistry, Vol. 2; Lipkowitz, K. B.; Boyd, D. B., Eds.; VCH: New York, 1991, p. 313.
17. Pople, J. A.; Beveridge, D. L. Approximate Molecular Orbital Theory; McGraw-Hill: New York, 1970.
18. Löwdin, P. O. J Chem Phys 1950, 18, 365.
19. Szabo, A.; Ostlund, N. S. Modern Quantum Chemistry: Introduction to Advanced Electronic Structure Theory; McGraw-Hill: New York, 1989.
20. Biegler, F. W.; Nguyen-Dang, T. T.; Tal, Y.; Bader, R. F. W.; Duke, A. J. J Phys B 1981, 14, 2739.
21. Bader, R. F. W. Atoms in Molecules: A Quantum Theory; Oxford University Press: Oxford, UK, 1990.
22. Mayer, I. Int J Quantum Chem 1986, 29, 73.
23. Mayer, I. Int J Quantum Chem 1986, 29, 477.
24. Noodleman, L.; Norman, J. G. Jr. J Chem Phys 1979, 70, 4903.
25. Noodleman, L. J Chem Phys 1981, 74, 5737.
26. Noodleman, L.; Davidson, E. R. Chem Phys 1986, 109, 131.
27. Löwdin, P. O. Phys Rev 1955, 97, 1509.
28. Löwdin, P. O. Rev Mod Phys 1960, 32, 328.
29. Löwdin, P. O. Quantum Theory of Atoms, Molecules, and the Solid State; Academic Press: New York, 1966.
30. Spiro, T. G., Ed. Iron–Sulfur Proteins; Wiley: New York, 1982.
31. Trautwein, A.; Bill, E.; Bominaar, E.; Winkler, H. Struct Bond 1991, 78, 1.
32. Dewar, M. J. S.; Zoebisch, E. G.; Healy, E. F.; Stewart, J. J. P. J Am Chem Soc 1985, 107, 3902.
33. Dewar, M. J. S.; Thiel, W. J Am Chem Soc 1977, 99, 4899.
34. Thiel, W. Tetrahedron 1988, 44, 7393.
35. Stewart, J. J. P. J Comput Chem 1989, 10, 209.
36. Stewart, J. J. P. J Comput Chem 1989, 10, 221.
37. Voityuk, A. A.; Zerner, M. C.; Rösch, N. J Phys Chem A 1999, 103, 4553.
38. Pople, J. A.; Santry, D. P.; Segal, G. A. J Chem Phys 1965, 43, S129.
39. Pople, J. A.; Segal, G. P. J Chem Phys 1965, 43, S136.
40. Pople, J. A.; Beveridge, D. L.; Dobosh, P. A. J Chem Phys 1967, 47, 2026.
41. Pariser, R.; Parr, R. G. J Chem Phys 1953, 21, 767.
42. Pariser, R.; Parr, R. G. J Chem Phys 1953, 21, 466.
43. Pople, J. A. Trans Faraday Soc 1953, 49, 1375.
44. Lykos, P.; Parr, R. G. J Chem Phys 1956, 24, 1166.
45. Wolfsberg, M.; Helmholz, L. J Chem Phys 1952, 20, 837.
46. Hoffmann, R. J Chem Phys 1963, 39, 1397.
47. Hoffmann, R. J Chem Phys 1964, 40, 2474.
48. Hoffmann, R. J Chem Phys 1964, 40, 2480.
49. Hoffmann, R. J Chem Phys 1964, 40, 2745.
50. Hoffmann, R. Tetrahedron 1966, 22, 521.
51. Hoffmann, R. Tetrahedron 1966, 22, 539.
52. Anderson, W. P.; Edwards, W. D.; Zerner, M. C. Inorg Chem 1986, 25, 2728.
53. Estiú, G. L.; Cory, M. G.; Zerner, M. C. J Phys Chem A 2000, 104, 233.
54. Estiú, G. L.; Zerner, M. C. J Phys Chem 1996, 100, 16874.
55. Estiú, G. L.; Zerner, M. C. J Phys Chem 1994, 98, 9972.
56. Stavrev, K. K.; Zerner, M. C. Chem Phys Lett 1996, 263, 667.
57. Stavrev, K. K.; Zerner, M. C. J Chem Phys 1995, 102, 34.
58. O'Brien, T. A.; Albert, K.; Zerner, M. C. J Chem Phys 2000, 113, 2203.
59. O'Brien, T. A.; Albert, K.; Zerner, M. C. J Chem Phys 2000, 112, 3192.
60. Boone, A. J.; Cory, M. G.; Scott, M. J.; Zerner, M. C.; Richards, N. G. J. Inorg Chem 2001, 40, 1837.
61. Zerner, M. C. Int J Quantum Chem 1989, 35, 567.
62. Boys, S. F. Rev Mod Phys 1960, 32, 296.
63. Boys, S. F. Rev Mod Phys 1960, 32, 300.
64. Boys, S. F. Rev Mod Phys 1960, 32, 306.
65. Boys, S. F. In Quantum Theory of Atoms, Molecules, and the Solid State; Löwdin, P.-O., Ed.; Academic Press: New York, 1966; p. 266.
66. Wieghardt, K.; Pohl, K.; Jibril, I.; Huttner, G. Angew Chem 1984, 96, 66.
67. Wieghardt, K.; Pohl, K.; Jibril, I.; Huttner, G. Angew Chem Int Ed Engl 1984, 23, 771.
68. Barra, A. L.; Debrunner, P.; Gatteschi, D.; Schulz, C. E.; Sessoli, R. Europhys Lett 1996, 35, 133.
69. Lis, T. Acta Crystallogr B 1980, 36, 2042.
70. Caneschi, A.; Gatteschi, D.; Sessoli, R.; Barra, A.-L.; Brunel, L. C.; Guillot, M. J Am Chem Soc 1991, 113, 5873.
71. Sessoli, R.; Tsai, H.-L.; Schake, R.; Wang, S.; Vincent, J. B.; Folting, K.; Gatteschi, D.; Christou, G.; Hendrickson, D. N. J Am Chem Soc 1993, 115, 1804.
72. Eppley, H. J.; Tsai, H.-L.; de Vries, N.; Folting, K.; Christou, G.; Hendrickson, D. N. J Am Chem Soc 1995, 117, 301.
73. Sun, Z. J.; Ruiz, D.; Rumberger, E.; Incarvito, C. D.; Folting, K.; Rheingold, A. L.; Christou, G.; Hendrickson, D. N. Inorg Chem 1998, 37, 4758.
74. Aubin, S. M. J.; Spagna, S.; Eppley, H. J.; Sager, R. E.; Christou, G.; Hendrickson, D. N. Chem Commun 1998, 803.
75. Aromi, G.; Aubin, S. M. J.; Bolcar, M. A.; Christou, G.; Eppley, H. J.; Folting, K.; Hendrickson, D. N.; Huffman, J. C.; Squire, R. C.; Tsai, H.-L.; Wang, S.; Wemple, M. W. Polyhedron 1998, 17, 3005.
76. Press, W. H.; Teukolsky, S. A.; Vetterling, W. T.; Flannery, B. P. Numerical Recipes in Fortran 77: The Art of Scientific Computing, 2nd ed.; Cambridge University Press: Cambridge, UK, 1992.
77. Anderson, E.; Bai, Z.; Bischof, C.; Blackford, S.; Demmel, J.; Dongarra, J.; Du Croz, J.; Greenbaum, A.; Hammarling, S.; McKenney, A.; Sorensen, D. LAPACK Users' Guide, 3rd

ed.; Society for Industrial and Applied Mathematics: Philadelphia, 1999.
78. Hyperchem—Release 5.1 Pro for Windows; Hypercube, Inc.: Gainesville, FL, 1997.
79. Walsh, C. Enzymatic Reaction Mechanisms; W. H. Freeman: San Francisco, 1979.
80. Burgess, B. K. Chem Rev 1990, 90, 1337.
81. Lippard, S. J. Angew Chem Int Ed Engl 1988, 27, 344.
82. McCusker, J. K.; Vincent, J. B.; Schmitt, E. A.; Mino, M. L.; Shin, K.; Coggin, D. K.; Hagen, P. M.; Huffman, J. C.; Christou, G.; Hendrickson, D. N. J Am Chem Soc 1991, 113, 3012.
83. Gorun, S. G.; Papaefthymiou, G. C.; Frankel, R. B.; Lippard, S. J. J Am Chem Soc 1987, 109, 4244.
84. Christmas, C. A.; Tsai, H.-L.; Pardi, L.; Kesselman, J. M.; Gantzel, P. K.; Chadha, R. K.; Gatteschi, D.; Harvey, D. F.; Hendrickson, D. N. J Am Chem Soc 1993, 115, 12483.
85. Crichton, R. R. Angew Chem Int Ed Engl 1973, 12, 57.
86. Theil, E. C. Annu Rev Biochem 1987, 56, 289.
87. Averill, B. A.; Davis, J. C.; Burman, S.; Zirino, T.; Sanders-Loehr, J.; Loehr, T. M.; Sage, J. T.; Debrunner, P. G. J Am Chem Soc 1987, 109, 3760.
88. Mann, S.; Bannister, J. V.; Williams, R. J. P. J Mol Biol 1986, 188, 225.
89. Smith, J. M. A.; Helliwell, J. R. Inorg Chim Acta 1985, 106, 193.
90. Theil, E. C. Adv Inorg Biochem 1983, 5, 1.
91. Armstrong, W. H.; Roth, M. E.; Lippard, S. J. J Am Chem Soc 1987, 109, 6318.
92. Chaudhuri, P.; Winter, M.; Fleischhauer, P.; Haase, W.; Florke, U.; Haupt, H.-J. Inorg Chim Acta 1993, 212, 241.
93. Wu, L.; Pressprich, M.; Coppens, P.; DeMarco, M. J. Acta Crystallogr C 1993, 49, 1255.
94. Gorun, S. M.; Lippard, S. J. Inorg Chem 1988, 27, 149.
95. Vincent, J. B.; Christmas, C.; Huffman, J. C.; Christou, G.; Chang, H.-R.; Hendrickson, D. N. J Chem Soc Chem Commun 1987, 236.
96. Vincent, J. B.; Christmas, C.; Chang, H.-R.; Li, Q.; Boyd, P. D. W.; Huffman, J. C.; Hendrickson, D. N.; Christou, G. J Am Chem Soc 1989, 111, 2086.
97. Libby, E.; McCusker, J. K.; Schmitt, E. A.; Folting, K.; Hendrickson, D. N.; Christou, G. Inorg Chem 1991, 30, 3486.
98. Bouwman, E.; Bolcar, M. A.; Libby, E.; Huffman, J. C.; Folting, K.; Christou, G. Inorg Chem 1992, 31, 5185.
99. Wemple, M. W.; Tsai, H.-L.; Wang, S.; Claude, J.-P.; Streib, W. E.; Huffman, J. C.; Hendrickson, D. N.; Christou, G. Inorg Chem 1996, 35, 6437.
100. Chandra, S. K.; Chakraborty, P.; Chakravorty, A. J Chem Soc Dalton Trans 1993, 863.
101. Mikuriya, M.; Yamoto, Y.; Tokii, T. Chem Lett 1991, 1429.
102. Gedye, C.; Harding, C.; McKee, V.; Nelson, J.; Patterson, J. J Chem Soc Chem Commun 1992, 392.
103. Thorp, J. J.; Sarneski, J. E.; Kulawiec, R. J.; Brudvig, G. W.; Crabtree, R. H.; Papaefthymiou, G. C. Inorg Chem 1991, 30, 1153.
104. Bino, A.; Chayat, R.; Pedersen, E.; Schneider, A. Inorg Chem 1991, 30, 856.
105. Ellis, T.; Glass, M.; Harton, A.; Folting, K.; Huffman, J. C.; Vincent, J. B. Inorg Chem 1994, 33, 5522.
106. Castro, S. L.; Sun, Z.; Bollinger, J. C.; Hendrickson, D. N.; Christou, G. J Chem Soc Chem Commun 1995, 2517.
107. Wemple, M. W.; Coggin, D. K.; Vincent, J. B.; McCusker, J. K.; Streib, W. E.; Huffman, J. C.; Hendrickson, D. N.; Christou, G. J Chem Soc Dalton Trans 1998.
108. Barra, A. L.; Caneschi, A.; Cornia, A.; Fabrizi de Biani, F.; Gateschi, D.; Sangregorio, C.; Sessoli, R.; Sorace, L. J Am Chem Soc 1999, 121, 5302.
109. Gorun, S. M.; Lippard, S. J. Inorg Chem 1991, 30, 1625.
110. Weihe, H.; Gudel, H. U. J Am Chem Soc 1997, 119, 6539.
111. Murray, K. Adv Inorg Chem 1995, 43, 261.
112. McCusker, J. K.; Christmas, C. A.; Hagan, P. M.; Chadha, R. K.; Harvey, D. F.; Hendrickson, D. N. J Am Chem Soc 1991, 113, 6114.
113. Harvey, D. F.; Christmas, C. A.; McCusker, J. K.; Hagan, P. M.; Chadha, R. K.; Hendrickson, D. N. Agnew Chem Int Ed Engl 1991, 30, 598.
114. Seddon, E. J.; Huffman, J. C.; Christou, G. J Chem Soc Dalton Trans 2000, 4446.
115. Zeng, Z.; Duan, Y.; Guenzburger, D. Phys Rev B 1997, 55, 12522.